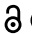



RESEARCH PAPER

 OPEN ACCESS 

ATF3 -activated accelerating effect of LINC00941/IncIAPF on fibroblast-to-myofibroblast differentiation by blocking autophagy depending on ELAVL1/HuR in pulmonary fibrosis

Jinjin Zhang^{a,b,*}, Haixia Wang^{a,c,*}, Hongbin Chen^{a,r}, Hongbo Li^c, Pan Xu^c, Bo Liu^c, Qian Zhang^d, Changjun Lv^c, and Xiaodong Song^{a,c}

^aDepartment of Cellular and Genetic Medicine, School of Pharmaceutical Sciences, Binzhou Medical University, Yantai, Shandong, China; ^bMedical Research Center, Binzhou Medical University, Yantai, Shandong, China; ^cDepartment of Respiratory and Critical Care Medicine, Binzhou Medical University Hospital, Binzhou Medical University, Binzhou, Province, China; ^dDepartment of Pathology, Binzhou Medical University Hospital, Binzhou Medical University, Binzhou, Province, China

ABSTRACT

Idiopathic pulmonary fibrosis (IPF) is characterized by lung scarring and has no effective treatment. Fibroblast-to-myofibroblast differentiation and myofibroblast proliferation and migration are major clinical manifestations of this disease; hence, blocking these processes is a practical treatment strategy. Here, highly upregulated *LINC00941/IncIAPF* was found to accelerate pulmonary fibrosis by promoting fibroblast-to-myofibroblast differentiation and myofibroblast proliferation and migration. Assay for transposase-accessible chromatin using sequencing and chromatin immunoprecipitation experiments elucidated that histone 3 lysine 27 acetylation (H3K27ac) activated the chromosome region opening in the *LINC00941* promoter. As a consequence, the transcription factor ATF3 (activating transcription factor 3) bound to this region, and *LINC00941* transcription was enhanced. RNA affinity isolation, RNA immunoprecipitation (RIP), RNase-RIP, half-life analysis, and ubiquitination experiments unveiled that *LINC00941* formed a RNA-protein complex with ELAVL1/HuR (ELAV like RNA binding protein 1) to exert its pro-fibrotic function. Dual-fluorescence mRFP-GFP-MAP1LC3/LC3 (microtubule associated protein 1 light chain 3) adenovirus monitoring technology, human autophagy RT² profiler PCR array, and autophagic flux revealed that the *LINC00941*-ELAVL1 axis inhibited autophagosome fusion with a lysosome. ELAVL1 RIP-seq, RIP-PCR, mRNA stability, and rescue experiments showed that the *LINC00941*-ELAVL1 complex inhibited autophagy by controlling the stability of the target genes *EZH2* (enhancer of zeste 2 polycomb repressive complex 2 subunit), *STAT1* (signal transducer and activators of transcription 1) and *FOXK1* (forkhead box K1). Finally, the therapeutic effect of *LINC00941* was confirmed in a mouse model and patients with IPF. This work provides a therapeutic target and a new effective therapeutic strategy related to autophagy for IPF.

Abbreviations: ACTA2/a-SMA: actin alpha 2, smooth muscle; ATF3: activating transcription factor 3; ATG: autophagy related; Baf-A1: bafilomycin A₁; BLM: bleomycin; CDKN: cyclin dependent kinase inhibitor; CLN3: CLN3 lysosomal/endosomal transmembrane protein, battenin; COL1A: collagen type I alpha; COL3A: collagen type III alpha; CXCR4: C-X-C motif chemokine receptor 4; DRAM2: DNA damage regulated autophagy modulator 2; ELAVL1/HuR: ELAV like RNA binding protein 1; EZH2: enhancer of zeste 2 polycomb repressive complex 2 subunit; FADD: Fas associated via death domain; FAP/FAPα: fibroblast activation protein alpha; FOXK1: forkhead box K1; FVC: forced vital capacity; GABARAP: GABA type A receptor-associated protein; GABARAPL2: GABA type A receptor associated protein like 2; IGF1: insulin like growth factor 1; IPF: idiopathic pulmonary fibrosis; LAMP: lysosomal associated membrane protein; lncRNA: long noncoding RNA; MAP1LC3/LC3: microtubule associated protein 1 light chain 3; NPC1: NPC intracellular cholesterol transporter 1; RGS: regulator of G protein signaling; RPLP0: ribosomal protein lateral stalk subunit P0; ROC: receiver operating characteristic; S100A4: S100 calcium binding protein A4; SQSTM1/p62: sequestosome 1; STAT1: signal transducers and activators of transcription 1; TGFβ1/TGF-β1: transforming growth factor beta 1; TNF: tumor necrosis factor; UIP: usual interstitial pneumonia; ULK1: unc-51 like autophagy activating kinase 1; VIM: vimentin.

ARTICLE HISTORY


Received 21 April 2021
Revised 11 February 2022
Accepted 22 February 2022

KEYWORDS

Autophagy; EZH2; fibroblast-to-myofibroblast differentiation; FOXK1; ELAVL1; lncRNA; myofibroblast proliferation and migration; pulmonary fibrosis; STAT1

CONTACT Xiaodong Song  songxd71@163.com  Department of Cellular and Genetic Medicine, School of Pharmaceutical Sciences, Binzhou Medical University, Yantai 264003, Shandong, China; Changjun Lv  lucky_lcj@sina.com  Department of Respiratory and Critical Care Medicine, Binzhou Medical University Hospital, Binzhou Medical University

*These authors contributed equally to this work.

 Supplemental data for this article can be accessed [here](#)

© 2022 The Author(s). Published by Informa UK Limited, trading as Taylor & Francis Group.
This is an Open Access article distributed under the terms of the Creative Commons Attribution-NonCommercial-NoDerivatives License (<http://creativecommons.org/licenses/by-nc-nd/4.0/>), which permits non-commercial re-use, distribution, and reproduction in any medium, provided the original work is properly cited, and is not altered, transformed, or built upon in any way.

Introduction

Idiopathic pulmonary fibrosis (IPF) is generally defined as a specific form of chronic, progressive, fibrosing interstitial pneumonia of unknown cause with the histopathological and/or radiological pattern of usual interstitial pneumonia (UIP) [1]. Raghu proposed the acceptance of IPF as a manifestation of irreversible pulmonary fibrosis of many entities that is caused by several occult or overt causative factors, including genetics, sex, age, intrinsic and extrinsic environmental factors, and systemic factors. This proposal is in contrast to the notion that IPF is a specific entity characterized by UIP of unknown cause [2]. The renewal of this concept may change the clinical diagnosis and treatment strategy of IPF and highlight the process of pulmonary fibrosis. Thus, understanding how fibroblast-to-myofibroblast differentiation causes uncontrolled proliferation and high myofibroblast migration and extracellular matrix deposition leading to pulmonary fibrogenesis is necessary.

Long noncoding RNAs (lncRNAs) belong to a class of regulatory noncoding RNAs that have a length more than 200 nt and are usually unable to code protein but can control multiple biological processes [3]. Their regulatory functions mainly depend on distinct processing and different subcellular localizations. For example, lncRNA *FAST* orthologs exhibit different subcellular localization in human embryonic stem cells (HsESCs) and murine ESCs (MmESCs) because of differential RNA processing. In HsESCs, cytoplasm-localized Hs*FAST* binds to the WD40 domain of the E3 ubiquitin ligase BTRC/b-TrCP and blocks its interaction with phosphorylated CTNNB1/b-catenin to prevent degradation. As a result, WNT signaling, which is required for pluripotency, is activated. By contrast, Mm*FAST* is retained in the nucleus of MmESCs, and its processing is suppressed by the splicing factor PPIE, which is highly expressed in MmESCs but not HsESCs [4]. Further study on these differentially expressed lncRNAs may provide a novel approach for the diagnosis and treatment of certain diseases. The prostate-specific lncRNAs of *PCA3* (prostate cancer associated 3) and *PCGEM1* (PCGEM prostate-specific transcript) detected in urine or blood have been used to differentiate prostate tumor and normal tissues and have diagnostic specificity and sensitivity of 83% and 67%, respectively, relative to those from the biopsy data [5]. The fat-specific lncRNA *Lep/Ob* controls the quantitative expression of the *Lep* (leptin) gene, and its defects can lead to a hypoleptinemic form of obesity that is responsive to LEP treatment [6]. In fibrosis, many lncRNAs are involved in various organs fibrosis, such as the liver, lung, heart and kidney. The profibrotic lncRNA *NONMMUT022555/lncRNA PFL* contributes to cardiac fibrosis by functioning as a competing endogenous RNA of *MIRLET7D/let-7d* [7]. LncRNA *H19*-mediated M2 polarization of macrophages promotes myofibroblast differentiation in pulmonary fibrosis induced by arsenic exposure [8]. LncRNA *ErbB4-IR* (intron region) contributes to TGFB1/TGF- β 1 (transforming growth factor beta 1)-SMAD3 (SMAD family member 3)-mediated renal fibrosis via downregulating SMAD7 (SMAD family member 7) [9]. In general, the study of lncRNAs associated with

fibrosis, particularly pulmonary fibrosis, is only in the preliminary stage.

Our previous studies revealed that different lncRNAs regulate pulmonary fibrogenesis in different cell types. *LncITPF* (a novel lncRNA renamed by its function) forms an RNA-protein complex with HNRNPL (heterogeneous nuclear ribonucleoprotein L) to control its host gene *ITGBL1* in fibroblasts, thus accelerating lung fibrosis. LncRNA *BC158825/LncPCF* promotes pulmonary fibrosis by sponging microRNA (miRNA) *Mir344-5p* to target MAP3K11 in alveolar epithelial cells [10–12]. However, the regulatory mechanism of lncRNA on cellular differentiation remains largely unknown. In the present work, whole-transcriptome analysis was performed to screen differentially expressed lncRNAs in human lung fibroblasts. The upregulated RNA transcript of *LINC00941/lncIAPF* was further investigated. Recent research showed that *LINC00941* promotes proliferation and invasion of colon cancer by acting on the *MIR205-5p-MYC* axis as a ceRNA mechanism [13]. However, its upregulation mechanism and the underlying mechanism by sequestering RNA-binding protein (RBP) remain largely unknown. Here, highly expressed *LINC00941* regulation on fibroblast-to-myofibroblast differentiation through sequestering RBP to target macroautophagy/autophagy process and its potential clinical relevance in patients with IPF was further explored. Due to its inhibitory function on autophagy, we renamed *LINC00941* as *lncIAPF* (Inhibit Autophagy in Pulmonary Fibrogenesis). The findings can provide a diagnostic biomarker in blood, or a potential therapeutic target related to autophagy for IPF.

Results

Mechanism of LINC00941/lncIAPF upregulation in pulmonary fibrosis

TGFB1 was used to activate fibroblast differentiation into myofibroblast in human fetal lung fibroblast MRC-5 cell. Whole-transcriptome sequencing was first conducted to test the differentially expressed lncRNAs in normal MRC-5 cells and MRC-5 cells activated with TGFB1 for 72 h. *LINC00941* RNA transcript had markedly higher expression than other RNAs (Figure 1A,B). With the use of Affymetrix Human Transcriptome Array 2.0 microarray, *LINC00941* was found to have the highest expression among lncRNAs and the highest co-expression degree with the mRNAs of fibrotic markers [14] and thus selected for further investigation. For sequencing data confirmation, *lncIAPF* expression was assessed in MRC-5 cells activated with TGFB1 for 0, 6, 12, 24, 48 and 72 h. qRT-PCR results reflected that *lncIAPF* was upregulated (Figure 1C). Afterward, 5'- and 3'-rapid amplification of complementary DNA ends (RACE) experiment was performed to analyze the full-length sequence of *lncIAPF*. The results uncovered that *lncIAPF* has 1967 base pairs in length (Fig. S1A). The protein-coding ability scores of *lncIAPF* were evaluated using the following tools: Coding Potential Calculator (<http://cpc.cbi.pku.edu.cn/>) and Coding Potential Assignment Tool (<http://lilab.research.bcm.edu/cpat/index.php>). The

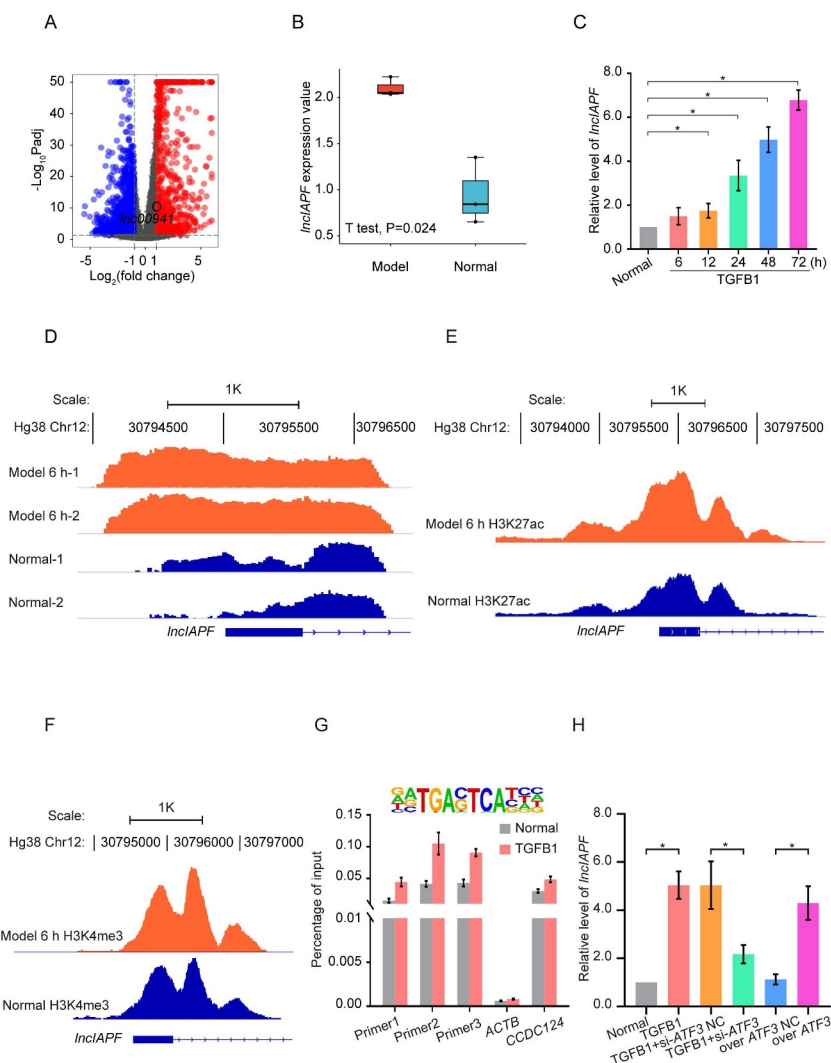


Figure 1. Highly expressed mechanism of *LINC00941/InclAPF*. (A) Whole-transcriptome sequencing tested the differentially expressed lncRNAs in normal MRC-5 cells and MRC-5 activated with TGFB1 for 72 h. *LINC00941* RNA transcript had markedly higher expression. (B) qRT-PCR confirmed the highly expressed *InclAPF* RNA transcript in the samples used for whole-transcriptome sequencing. (C) qRT-PCR results showed that *InclAPF* was upregulated in MRC-5-treated with TGFB1 for 0, 6, 12, 24, 48 and 72 h. (D) Gene tracking of ATAC-seq signal for *InclAPF* after TGFB1 treatment for MRC-5 cells for 6 h revealed that TGFB1 increased the chromatin accessibility in the *InclAPF* promoter compared with that in the normal group. 1 K indicates the length of *InclAPF* promoter, and Hg38 indicates the human reference genome. (E) ChIP-seq revealing a significant H3K27ac modification peak in the transcription start sites of *InclAPF* in each group. Significant difference in peak value was found between the TGFB1-treated and normal groups. (F) ChIP-seq indicating significant H3K4me3 modification peak in the transcription start sites of *InclAPF* in each group. No significant difference in peak value was found between the TGFB1-treated and normal groups. (G) Motif analysis of ATF3 binding site with *InclAPF* promoter (above). ChIP-purified DNA targeting of the indicated genes analyzed by qPCR revealed ATF3 binding at the *InclAPF* promoter region with or without TGFB1 treatment. Primers 1–3 were designed for *InclAPF* promoter. ACTB/ β -actin was used as negative control. Human ortholog coiled-coil domain containing 124 (CCDC124) was used as positive control. (H) qRT-PCR showed that si-ATF3 reduced *InclAPF* expression, and overexpressed ATF3 increased *InclAPF*. Each bar represents the mean \pm SD; n = 6; *p < 0.05.

scores were 0.187173 and 0.1735537, respectively, indicating that *InclAPF* was devoid of protein-coding potential. In the UCSC and Ensemble databases, *InclAPF* was also annotated as a lncRNA.

Subsequently, the factor underlying the considerable increase in *InclAPF* expression in lung fibrosis was investigated. Chromatin undergoes dynamic, organizational changes in normal or disease state; hence, an assay for transposase-accessible chromatin using sequencing (ATAC-seq) was performed to test chromosome-region opening during pulmonary fibrosis [15]. Considering that chromosome-region opening occurs prior to gene expression, normal cells and those treated with TGFB1 for 6 h were tested.

ATAC-seq findings revealed that TGFB1 considerably increased the chromosome opening peak in *InclAPF* promoter compared with that in the normal group (Figure 1D). This result indicated that *InclAPF* transcription is more active in the TGFB1-treated group than in the normal group. Chromatin immunoprecipitation (ChIP)-seq was then performed to study histone modification. Significant histone H3 lysine 4 trimethylation (H3K4me3) and H3K27ac modification peaks were found near the transcription start sites of *InclAPF* in each group. Significant difference was found in the H3K27ac modification peak (Figure 1E) but not in the peak value of H3K4me3 (Figure 1F) between the TGFB1-treated and normal groups.

Therefore, the differential expression of *lncIAPF* was related to H3K27ac modification but not to H3K4me3 modification. Further analysis was performed on the transcription factors that specifically bound to *lncIAPF* promoter. ATF3 ranked first according to p values based on ATAC-seq and hence was selected for further study. After the motif analysis of the ATF3 binding site, ChIP was performed to confirm the binding between ATF3 and *lncIAPF* promoter (Figure 1G). qRT-PCR results verified that ATF3 knock-down markedly reduced *lncIAPF* expression and vice-versa (Figure 1H). These findings indicated that H3K27ac modification contributes to chromosome-region opening in *lncIAPF* promoter. After chromosome-region opening, ATF3 binds to *lncIAPF* promoter and initiates *lncIAPF*

transcription. It may be one of the reasons that *lncIAPF* upregulates in pulmonary fibrosis.

lncIAPF accelerated pulmonary fibrogenesis by promoting fibroblast-to-myofibroblast differentiation

The smart silencer consisting of six RNA interference sites (si-*lncIAPF*) and overexpression vector (recombinant plasmid, RP) of *lncIAPF* were designed and transfected into MRC-5 cells to investigate *lncIAPF* function. The effects of si-*lncIAPF* and RP on fibroblast-to-myofibroblast differentiation were assessed by cell shape, differentiation-related proteins, fibrotic protein markers, and myofibroblast proliferation and migration. Real-time cellular analysis system manifested that

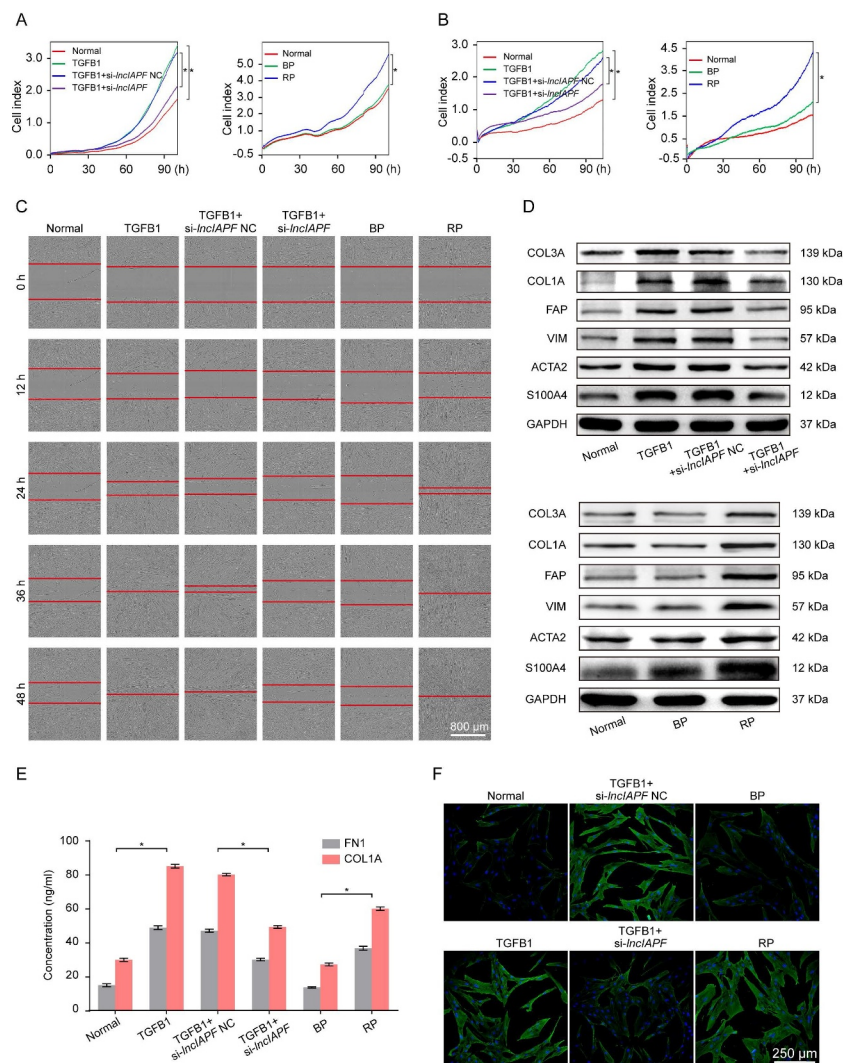


Figure 2. Pro-fibrotic function of *lncIAPF*. (A) Real-time cellular analysis system reflected that myofibroblast proliferation was slowed by the *lncIAPF* smart silencer and enhanced by *lncIAPF* overexpression. (B) Real-time cellular analysis system reflected that myofibroblast migration was slowed by the *lncIAPF* smart silencer and enhanced by *lncIAPF* overexpression. (C) Wound-healing assay was automatically monitored with an IncuCyte S3 instrument under *lncIAPF* smart silencer and overexpression treatment. *lncIAPF* smart silencer blocked myofibroblast migration. Conversely, *lncIAPF* overexpression promoted myofibroblast migration. (D) Western blot results exhibited that ACTA2, COL1A, COL3A, VIM, FAP and S100A4 were highly upregulated by TGFB1. *lncIAPF* smart silencer inhibited the expression of ACTA2, COL1A, COL3A and VIM. Conversely, *lncIAPF* overexpression elevated the expression of ACTA2, COL1A, COL3A, VIM, FAP and S100A4. GAPDH served as the control. (E) Expression of COL1A and FN1 in the media of the cultured cells reduced by *lncIAPF* smart silencer and promoted by *lncIAPF* overexpression. (F) Immunofluorescence staining observed that cells became spindle-shaped, ACTA2 was increased, and cell proliferation was enhanced in the TGFB1-treated MRC-5 group compared with those in normal cells. *lncIAPF* smart silencer repressed ACTA2 and cell proliferation compared with those in the TGFB1-treated group. *lncIAPF* overexpression considerably increased the ACTA2 and cell proliferation. Blue indicates nucleus marked with DAPI. Green indicates ACTA2 in cytoplasm. NC indicates a negative control of si-*lncIAPF*, BP indicates blank plasmid, and RP indicates the recombinant plasmid of overexpressed *lncIAPF*. Each bar represents the mean \pm SD; n = 6; *p < 0.05.

myofibroblast proliferation and migration was considerably increased by *lncIAPF* overexpression but blocked by *lncIAPF* smart silencer compared with those in the TGF β 1-treated groups (Figure 2A, B). These results were further confirmed by scratch wound-healing assay (Figure 2C). Western blot analysis revealed that TGF β 1 rapidly increased the amount of fibrotic markers, including ACTA2/ α -SMA (actin alpha 2, smooth muscle), COL1A (collagen type I alpha), COL3A (collagen type III alpha), and VIM (vimentin), and differentiation-related proteins, including FAP/FAP α (fibroblast activation protein alpha) and S100A4 (S100 calcium binding protein A4). However, their expression was reduced by *lncIAPF* smart silencer and promoted by *lncIAPF* overexpression (Figure 2D). Expression of COL1A and FN1 (fibronectin 1) in the media of the cultured cells also reduced by *lncIAPF* smart silencer and promoted by *lncIAPF* overexpression (Figure 2E). Immunofluorescence staining images depicted that the TGF β 1-treated fibroblasts appeared in a spindle shape and had strong proliferation and migration

abilities and rapidly increased ACTA2. *lncIAPF* overexpression had the same effect as TGF β 1. Meanwhile, *lncIAPF* smart silencer weakened the proliferation and migration abilities and decreased ACTA2 (Figure 2F). All these results suggest that *lncIAPF* is a pro-fibrotic factor that can accelerate pulmonary fibrosis by promoting fibroblast differentiation into myofibroblasts and myofibroblast proliferation and migration.

Regulatory mechanism of *lncIAPF* on the binding protein ELAVL1

LncRNA can form an RNA-protein complex with its binding protein to exert certain functions. Hence, RNA affinity isolation, protein mass spectrometry, and western blot analyses were performed to search for the binding protein of *lncIAPF* by dividing its full-length sequence into two sections, namely, 1–1017 and 1005–1895 nt sections. After segmentation, high-quality RNA transcriptions were obtained (Figure 3A). Silver

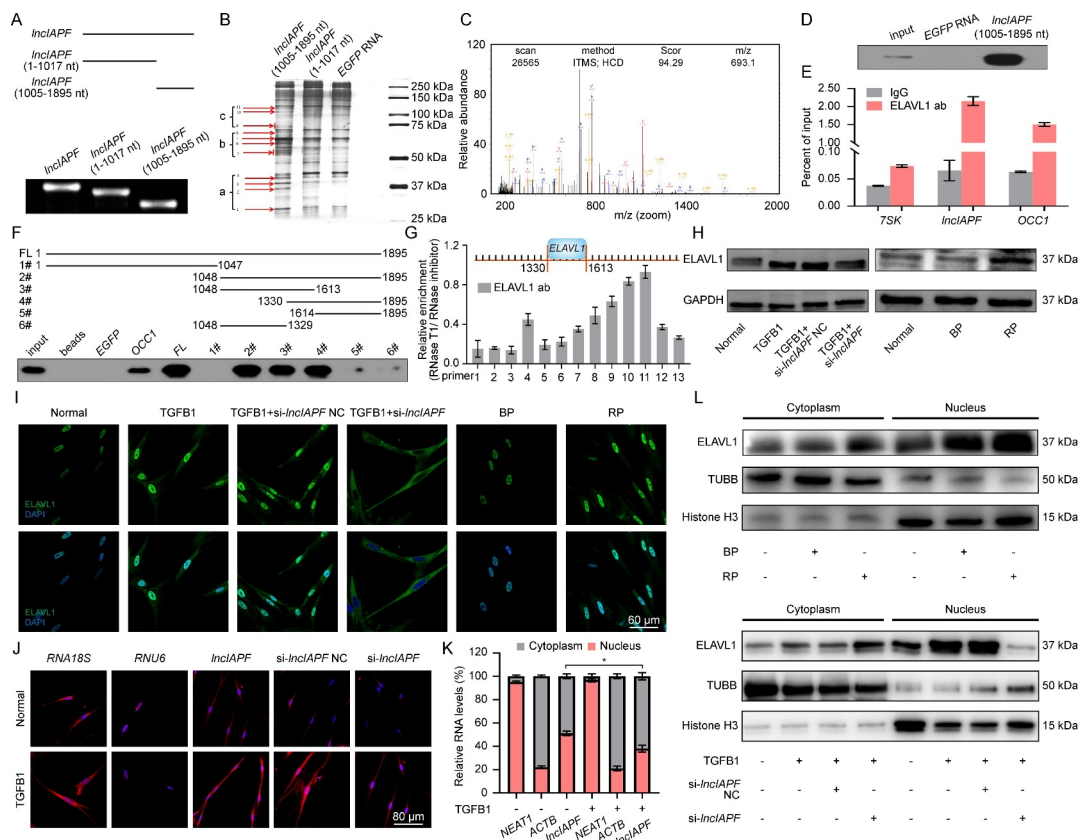


Figure 3. Identification of *lncIAPF* and its binding protein ELAVL1. (A) *lncIAPF* was divided into two sections, namely, 1–1017 nt and 1005–1895 nt (above) verified with high quality (below). (B) Silver staining indicated the *lncIAPF*-bound proteins from RNA affinity isolation in 1–1017 and 1005–1895 nt sections compared with those in the *EGFP* RNA group. Red arrow showed that 1005–1895 nt section had many differently expressed protein binds compared with the control. This section was divided into a, b, and c groups for further mass spectrometry analysis. (C) Mass spectrometry validated that ELAVL1 was the binding protein of *lncIAPF*. (D) Western blot results revealed that ELAVL1 was the binding protein of *lncIAPF*. (E) RIP results verified that ELAVL1 specifically concentrated large quantities of *lncIAPF*. *RN7SK* RNA served as negative control, *lncRNA OCC1* as positive control. (F) Full length 1005–1895 nt (FL) was further divided into 6 sections: 1[#] 1005–1047, 2[#] 1048–1895, 3[#] 1048–1613, 4[#] 1330–1895, 5[#] 1614–1895 and 6[#] 1048–1329. The RNA affinity isolation showed that ELAVL1 blot appeared in 2[#], 3[#], and 4[#] sections which shared the same sequence 1330–1613 section. (G) RNase-RIP experiments showed 9[#], 10[#], and 11[#] primers amplification regions of *lncIAPF* combined with ELAVL1. This region was in 1330–1613 nt of *lncIAPF*. 13 pairs of primers were designed for *lncIAPF* full length. (H) Western blot results showed that ELAVL1 expression increased/decreased under over-expressed/knockdown *lncIAPF* action. (I) Immunofluorescence results illustrated that ELAVL1 expression was increased by *lncIAPF* overexpression and decreased by *lncIAPF* knockdown. (J) Images of RNA FISH revealed that *lncIAPF* was located in the nucleus and cytoplasm. After TGF β 1 treatment, a small amount of *lncIAPF* translocated from the nucleus to cytoplasm. (K) Nuclear and cytosolic fraction confirmed that *lncIAPF* was present in the nucleus and cytoplasm. *Neat1* was primarily found in the nucleus, and *Actb* was primarily located in the cytoplasm. (L) Nuclear and cytosolic fraction exhibited that ELAVL1 was mainly located in the nucleus in normal cells. TGF β 1 and *lncIAPF* overexpression promoted minimal ELAVL1 translocation from the nucleus to cytoplasm, and *lncIAPF* knockdown reduced the total amount of ELAVL1 protein but did not trigger nucleocytoplasmic translocation. Each bar represents the mean \pm SD; n = 6; *p < 0.05.

staining was performed to detect *lncIAPF*-bound proteins from RNA pull-down. Staining images depicted that the active functional domain was in the 1005–1895 nt section, and the 1–1017 nt section had no differently expressed protein compared with the control (Figure 3B). The *lncIAPF*-bound proteins were further analyzed by mass spectrometry. Considering the varying protein bands found in the 1005–1895 nt section, it was divided into a, b, and c groups for further mass spectrometry. The results preliminarily exhibited that ELAVL1 was the major *lncIAPF*-binding protein. Mass spectrometry and western blot findings confirmed their binding relation (Figure 3C,D). RNA immunoprecipitation (RIP) results also revealed that ELAVL1 was specifically enriched by *lncIAPF* to prove their binding relationship. LncRNA overexpressed in colon carcinoma-1 (OCC-1) serves as positive control because it is upregulated in a subset of colon carcinomas (Figure 3E) [16].

The 1005–1895 sequence of *lncIAPF* was further divided into six sections: 1005–1047, 1048–1895, 1048–1613, 1330–1895, 1614–1895, and 1048–1329 to identify the binding domain. RNA pull-down analysis showed that ELAVL1 blot appeared in three sections: 1048–1895, 1048–1613, and 1330–1895, indicating that the binding domain was approximately in the 1330–1613 section of *lncIAPF* (Figure 3F). For

confirmation, 13 pairs of primers for *lncIAPF* and RNase-RIP experiment were designed (Table S1). The RNase-RIP results showed that ELAVL1 anchored at the 9[#], 10[#], and 11[#] primers in the amplification region of *lncIAPF* (Figure 3G). This region was also located in 1330–1613 nt in *lncIAPF*. ELAVL1 expression was then assessed by western blot. When the duration of TGFβ1 treatment was increased from 0 to 72 h, its expression was higher compared with that in normal cells (Fig. S1B). Western blot and immunofluorescence results showed that ELAVL1 expression was increased by *lncIAPF* overexpression but reduced by *lncIAPF* knock-down (Figure 3H,I). Hence, ELAVL1 was selected for further study.

The underlying mechanism between *lncIAPF* and ELAVL1 was further explored. LncRNA location determines its regulatory mechanisms, such as the transcriptional or posttranscriptional modification of mRNA and protein activity modulation. Thus, RNA fluorescence in situ hybridization (RNA FISH) and nuclear-cytosol fractionation were performed to detect *lncIAPF* location. RNA FISH analysis revealed that *lncIAPF* was visible in the nucleus and cytoplasm (Figure 3J). Nuclear-cytosol fractionation revealed that after TGFβ1 treatment, only a small amount of *lncIAPF* translocated from the nucleus to cytoplasm (Figure 3K). ELAVL1 translocation was also detected. Primarily located

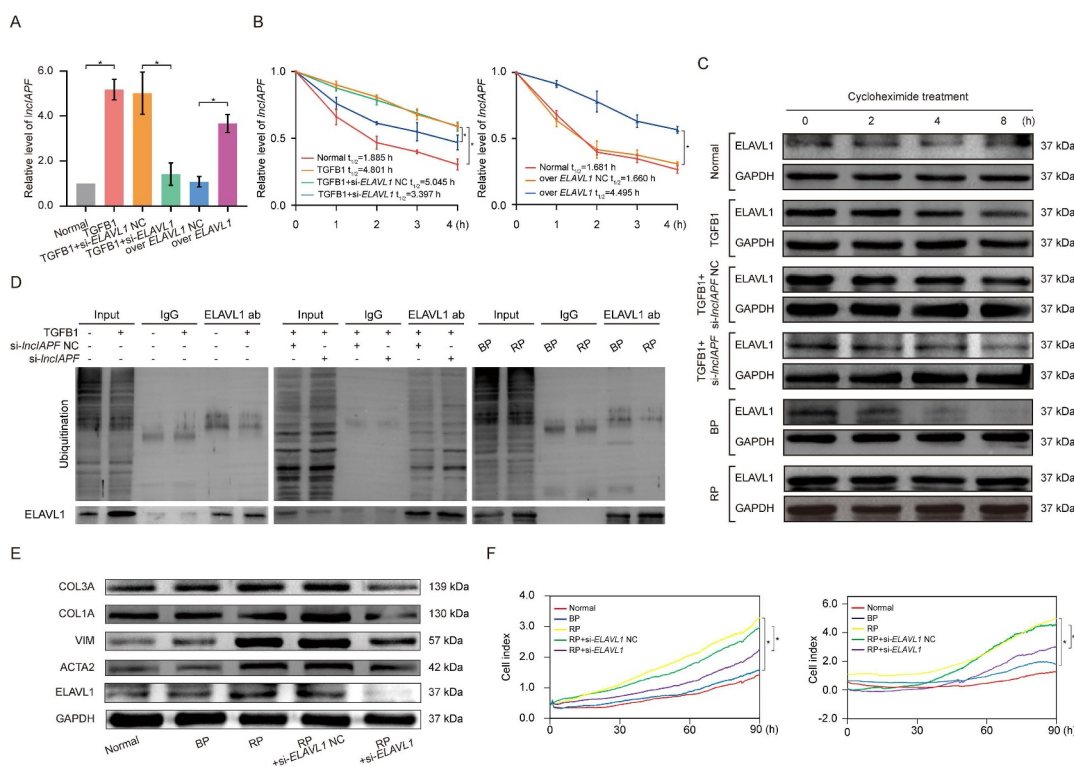


Figure 4. Effect of *lncIAPF* on fibrosis depends on ELAVL1. (A) qRT-PCR results showed that *lncIAPF* expression was increased by *ELAVL1* overexpression and reduced by *ELAVL1* knockdown. (B) Half-life of *lncIAPF* analysis unveiled that *lncIAPF* stability was enhanced by *ELAVL1* overexpression and reduced by *ELAVL1* knockdown. (C) Stability testing uncovered that *ELAVL1* stability was promoted by *lncIAPF* overexpression and decreased by *lncIAPF* knockdown. Half-life of each group was 5.96, 20.84, 18.99, 6.10, 6.63, 22.59 h in normal, TGFβ1, TGFβ1+ si-*lncIAPF* NC, TGFβ1+ si-*lncIAPF*, BP and RP group, respectively. (D) Ubiquitination experiments revealed *ELAVL1* ubiquitination was reduced by *lncIAPF* overexpression and enhanced by *lncIAPF* knockdown. (E) Rescue experiments elucidated that *lncIAPF* overexpression enhanced the expression of fibrotic proteins including ACTA2, VIM, and COL1A and COL3A. Interference of *ELAVL1* blocked these proteins' expression. (F) Rescue experiments manifested that *lncIAPF* overexpression promoted the myfibroblast proliferation and migration. Interference of *ELAVL1* expression caused their expression trends to be reversed. Each bar represents the mean ± SD; n = 6; *p < 0.05.

in the nucleus in normal cells, a small amount of ELAVL1 translocated from the nucleus to cytoplasm after TGF β 1 or overexpressed *IncIAPF* treatment. *IncIAPF* knockdown reduced the total amount of ELAVL1 protein but did not trigger its nucleocytoplasmic translocation (Figure 3L). ELAVL1 regulates numerous genes in the nucleus and cytoplasm through different mechanisms. We inferred that *IncIAPF* and ELAVL1 expression are affected by their stabilities, and not by their translocations. Hence, stability experiments were performed to explore the underlying mechanism. Gain- and loss-of-function studies revealed that *ELAVL1* overexpression increased *IncIAPF* level, and *ELAVL1* knockdown decreased *IncIAPF* expression (Figure 4A). Half-life of *IncIAPF* analysis indicated that *IncIAPF* stability was enhanced by *ELAVL1* overexpression but reduced by

ELAVL1 knockdown (Figure 4B). The stability of ELAVL1 protein was also measured by using cycloheximide experiments, and the results showed that ELAVL1 stability was enhanced by *IncIAPF* overexpression but reduced by *IncIAPF* knockdown (Figure 4C). Ubiquitination experiments also elucidated that *IncIAPF* overexpression decreased ELAVL1 ubiquitination, which led to ELAVL1 stability. *IncIAPF* knockdown promoted ELAVL1 ubiquitination, which resulted in ELAVL1 degradation (Figure 4D). The above results suggest that *IncIAPF* and ELAVL1 affect each other's stability. The rescue experiment showed that the levels of fibrotic markers such as ACTA2, VIM, COL1A and COL3A were increased by *IncIAPF* overexpression, but this effect was reversed by the interference of *ELAVL1* (Figure 4E). Myfibroblast proliferation and migration were enhanced by

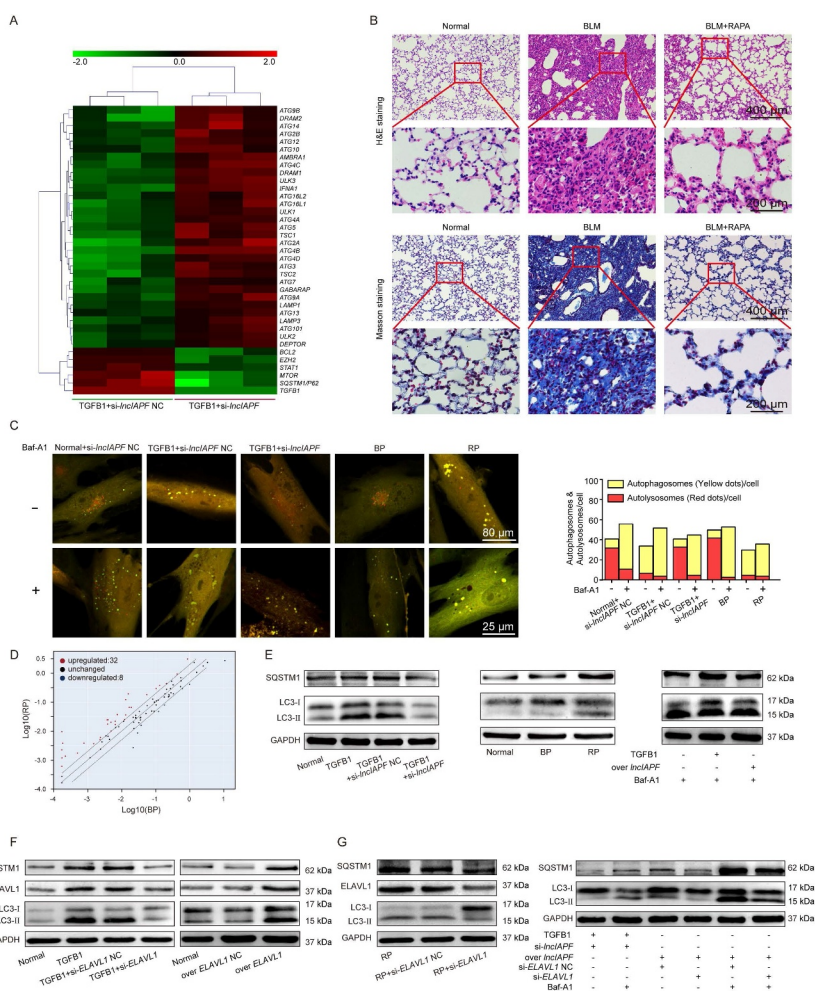


Figure 5. Effect of *IncIAPF* on autophagic flux depending on ELAVL1. (A) RNA sequencing was performed to test the differentially expressed mRNAs in TGF β 1+ knockdown *IncIAPF* NC and TGF β 1+ knockdown *IncIAPF* groups. Altered mRNAs were enriched in ATGs. Green to red indicated the low-to-high expression levels. (B) H&E and Masson images revealed that excess collagen was deposited and the alveolar wall became thicker in BLM group. Rapamycin alleviated fibrosis. (C) Dual-fluorescence mRFP-GFP-LC3 adenovirus monitoring technology was used to observe autophagy with the laser confocal microscope. The normal group emitted red and yellow fluorescence. TGF β 1-treated group emitted strong yellow fluorescence. The yellow fluorescence was enhanced in the overexpressed *IncIAPF*-treated group but weakened in the *IncIAPF* knockdown-treated group. The number of autophagosomes (GFP⁺mRFP⁺ spots) was increased, while the number of autolysosomes (GFP⁻mRFP⁺ spots) was decreased in Baf-A1 treatment groups compared with the non-treatment groups, respectively. (D) Human autophagy RT² profiler PCR array showed that *IncIAPF* overexpression caused changes in 84 ATGs. Red dot indicates the 32 upregulated ATGs; blue dot indicates the 8 downregulated ATGs; and black dot indicates the remaining 44 ATGs. (E) Western blot results revealed that LC3-II:LC3-I and SQSTM1 decreased in the normal group compared with those in the other groups. However, *IncIAPF* smart silence decreased LC3-II:LC3-I and SQSTM1 compared with those in the TGF β 1 group and *IncIAPF* overexpression increased LC3-II:LC3-I and SQSTM1. (F) LC3-II:LC3-I and SQSTM1 levels were decreased by si-*ELAVL1* but increased by *ELAVL1* overexpression. (G) Rescue experiments revealed that *IncIAPF* overexpression promoted the levels of autophagic proteins including LC3-II:LC3-I, and SQSTM1. After interfering with *ELAVL1* expression, these proteins' expression trends were reversed.

lncIAPF overexpression. However, these trends reversed by interference of *ELAVL1* expression (Figure 4F). Thus, the effect of *lncIAPF* on fibrosis depends on *ELAVL1*.

Inhibition of *lncIAPF-ELAVL1* complex on autophagy

Which signaling pathway is regulated by *lncIAPF*? Differentially expressed mRNAs were obtained in TGFB1 + knockdown *lncIAPF* NC and TGFB1+ knockdown *lncIAPF* groups by using RNA sequencing. GO analysis and functional enrichment of differential mRNA showed that *lncIAPF* regulation mainly enriched in autophagy signaling pathway. Some autophagy-related genes (ATGs) were up-regulated and some were down-regulated by knockdown *lncIAPF* (Figure 5A). Autophagy can function as a cytoprotector or deleterious effector to participate in the pathogenesis of pulmonary fibrosis [17]. Hence, the autophagy role was first studied in bleomycin (BLM)-treated mice model. The in vivo results indicated that excess collagen was deposited and the alveolar wall became thicker in BLM group. Rapamycin is known as autophagy inducer. H&E and Masson images revealed that rapamycin alleviated fibrosis (Figure 5B). The findings showed that autophagy can function as a cytoprotector in pulmonary fibrosis. For further illustration which stage of autophagy is blocked, real-time detection of tandem dual-fluorescence mRFP-GFP-LC3 adenovirus was performed to investigate the effects on autophagy by the knockdown and overexpression of *lncIAPF*. If autophagy is activated, then GFP green fluorescence will be quenched due to the decrease in pH value. Red fluorescence is still emitted even when the pH stability of mRFP red fluorescent is higher than that of GFP. Hence, red fluorescence indicates autolysosomes. Yellow fluorescence represents the co-localization of both GFP and mRFP fluorescence indicating the autophagosomes. This color indicates that the fusion proteins failed to completely fuse with lysosome, and autophagy is partially blocked. The percentage of yellow fluorescence spots reflects the autophagosome-lysosome fusion rate. So we used the IncuCyte S3 live-cell analysis system to observe the autophagy processes under various conditions. Videos of the whole autophagy process within 20 h in normal, TGFB1, overexpressed *lncIAPF*/NC and knockdown *lncIAPF*/NC groups were recorded as Supplementary Video. These videos vividly displayed the autophagy processes at different times for different groups. The videos showed that autophagosome formed normally and the fusion between autophagosome and lysosome was blocked in TGFB1 group. Overexpressed *lncIAPF* inhibited autophagy by blocking the fusion between autophagosome and lysosome, not blockade of autophagosome formation. Knockdown *lncIAPF* promoted the fusion between autophagosome and lysosome. Baf-A1 (Bafilomycin A₁) is an autophagy inhibitor, which can inhibit the fusion between autophagosome and lysosome and enhanced yellow fluorescence [18]. Therefore, Baf-A1 was added to confirm blockade of the fusion between autophagosome and lysosome, not autophagosome formation in TGFB1 and overexpressed *lncIAPF* groups, whereas knockdown of *lncIAPF* promoted the fusion between autophagosomes and lysosomes (Video S1–S4). Meanwhile, the images of fluorescence changes were

detected with the laser confocal microscope. Dual-fluorescence images revealed that the normal group emitted red and yellow fluorescence. The numbers of yellow fluorescence spots were markedly increasing in TGFB1 group compared with normal group. The yellow fluorescence was enhanced in the overexpressed *lncIAPF*-treated group but weakened in the *lncIAPF* knockdown-treated group. After adding Baf-A1, we observed a constant increase in the number of cells accumulating yellow fluorescence spots compared with every group without Baf-A1, which is suggestive of defective fusion of autophagosomes with lysosomes (Figure 5C). On the basis of the above findings, overexpressed

Table 1. The altered ATGs in overexpressed *lncIAPF* group.

Gene Symbol	Fold Regulation	Gene Symbol	Fold Regulation
<i>AMBRA1</i>	5.03	<i>IGF1</i>	2.44
<i>ATG10</i>	2.17	<i>LAMP1</i>	2.15
<i>ATG16L1</i>	9.32	<i>NPC1</i>	2.76
<i>ATG4B</i>	2.61	<i>RAB24</i>	2.55
<i>ATG4D</i>	4.18	<i>RGS19</i>	6.19
<i>ATG9A</i>	3.4	<i>SQSTM1</i>	2.2
<i>ATG9B</i>	3.48	<i>TGFB1</i>	12.39
<i>BCL2</i>	4.92	<i>TMEM74</i>	20.78
<i>BCL2L1</i>	4.89	<i>TNF</i>	12.93
<i>CASP3</i>	2.88	<i>TNFSF10</i>	4.51
<i>CDKN1B</i>	3.42	<i>ULK1</i>	6.54
<i>CLN3</i>	2.06	<i>ACTB</i>	3.59
<i>CTSS</i>	2.05	<i>ATG4C</i>	-2.39
<i>CXCR4</i>	55.24	<i>CDKN2A</i>	-3.43
<i>DAPK</i>	3.46	<i>DRAM2</i>	-2.28
<i>EIF4G1</i>	3.31	<i>GABARAP</i>	-2.41
<i>FADD</i>	4.0	<i>GABARAPL2</i>	-2.06
<i>FAS</i>	2.9	<i>PIK3C3</i>	-2.57
<i>HGS</i>	6.18	<i>SNCA</i>	-8.15
<i>IFNG</i>	6.77	<i>RPLP0</i>	-3.96

The positive number indicates upregulation and the negative number indicates downregulation.

Table 2. The altered ATGs in overexpressed *EZH2* group.

Gene Symbol	Fold Regulation	Gene Symbol	Fold Regulation
<i>AKT1</i>	2.52	<i>ATG3</i>	-6.50
<i>AMBR1</i>	5.24	<i>ATG4A</i>	-4.99
<i>ATG16L1</i>	2.43	<i>ATG4C</i>	-7.99
<i>ATG4B</i>	5.79	<i>ATG5</i>	-5.54
<i>ATG4D</i>	4.42	<i>ATG9B</i>	-2.64
<i>ATG9A</i>	8.37	<i>BID</i>	-2.26
<i>BAD</i>	3.01	<i>CASP3</i>	-7.22
<i>BAX</i>	2.56	<i>DRAM1</i>	-4.59
<i>BCL2L1</i>	5.94	<i>DRAM2</i>	-2.95
<i>CDKN1B</i>	2.21	<i>EIF2AK3</i>	-5.65
<i>CLN3</i>	4.88	<i>ESR1</i>	-8.69
<i>CTSD</i>	3.73	<i>FAS</i>	-7.10
<i>EIF4G1</i>	5.55	<i>GABARAP</i>	-2.54
<i>FADD</i>	3.97	<i>GABARAPL2</i>	-5.70
<i>GAA</i>	7.02	<i>HSP90AA1</i>	-4.79
<i>HDAC6</i>	3.94	<i>HSPA8</i>	-2.32
<i>HGS</i>	19.45	<i>IGF1</i>	-6.72
<i>HTT</i>	3.09	<i>IRGM</i>	-6.20
<i>LAMP1</i>	5.08	<i>MAP1LC3B</i>	-15.26
<i>NPC1</i>	3.84	<i>MAPK8</i>	-2.87
<i>RGS19</i>	4.13	<i>MTOR</i>	-2.22
<i>SQSTM1</i>	4.51	<i>PIK3C3</i>	-4.84
<i>TGFB1</i>	21.84	<i>PRKAA1</i>	-4.01
<i>TNFSF10</i>	5.00	<i>PTEN</i>	-10.41
<i>TP53</i>	2.39	<i>RB1</i>	-4.20
<i>ULK1</i>	5.33	<i>RPS6KB1</i>	-3.12
<i>ACTB</i>	4.09	<i>SNCA</i>	-18.35
<i>GAPDH</i>	2.84	<i>ULK2</i>	-2.07
<i>ATG10</i>	-5.18	<i>WIP1</i>	-3.17
<i>ATG12</i>	-5.12	<i>RPLP0</i>	-4.98

The positive number indicates upregulation and the negative number indicates downregulation.

Table 3. The altered ATGs in overexpressed *STAT1* group.

Gene Symbol	Fold Regulation	Gene Symbol	Fold Regulation
<i>AKT1</i>	5.58	<i>HDAC6</i>	9.44
<i>AMBRA1</i>	12.08	<i>HGS</i>	38.11
<i>APP</i>	4.54	<i>HTT</i>	6.80
<i>ATG10</i>	4.07	<i>INS</i>	1.87
<i>ATG16L1</i>	8.36	<i>LAMP1</i>	12.36
<i>ATG16L2</i>	4.05	<i>MAP1LC3A</i>	2.59
<i>ATG4A</i>	2.04	<i>MAPK14</i>	3.75
<i>ATG4B</i>	15.20	<i>MTOR</i>	2.38
<i>ATG4D</i>	8.53	<i>NFKB1</i>	3.16
<i>ATG5</i>	1.84	<i>NPC1</i>	10.19
<i>ATG7</i>	4.41	<i>PIK3CG</i>	5.43
<i>ATG9A</i>	16.83	<i>PIK3R4</i>	1.99
<i>BAD</i>	7.50	<i>PTEN</i>	2.17
<i>BAK1</i>	3.48	<i>RAB24</i>	1.92
<i>BAX</i>	6.68	<i>RGS19</i>	10.54
<i>BCL2</i>	2.24	<i>SNCA</i>	2.01
<i>BCL2L1</i>	15.08	<i>SQSTM1</i>	10.84
<i>BECN1</i>	3.69	<i>TGFB1</i>	39.72
<i>BID</i>	2.96	<i>TGM2</i>	2.78
<i>BNIP3</i>	2.51	<i>TNFSF10</i>	40.83
<i>CASP8</i>	4.01	<i>TP53</i>	7.92
<i>CDKN1B</i>	6.92	<i>ULK1</i>	9.67
<i>CDKN2A</i>	4.84	<i>ULK2</i>	2.58
<i>CLN3</i>	12.62	<i>UVRAG</i>	5.30
<i>CTSB</i>	3.71	<i>ACTB</i>	9.63
<i>CTSD</i>	8.00	<i>B2M</i>	17.00
<i>CTSS</i>	16.28	<i>GAPDH</i>	5.20
<i>EIF4G1</i>	10.25	<i>HPRT1</i>	2.69
<i>FADD</i>	17.12	<i>ATG9B</i>	-2.39
<i>FAS</i>	2.92	<i>ESR1</i>	-2.73
<i>GAA</i>	18.53	<i>IGF1</i>	-2.62
<i>GABARAPL1</i>	2.19	<i>IRGM</i>	-6.18
<i>HDAC1</i>	2.99		

The positive number indicates upregulation and the negative number indicates downregulation.

lncIAPF inhibits autophagy by blocking autophagosome fusion with lysosome, not blockade of autophagosome formation. Knockdown *lncIAPF* promotes autophagosome fusion with lysosome.

Subsequently, the 84 ATGs were analyzed using human autophagy RT² profiler PCR array. According to the expressed profiles of ATGs, 32 and 8 were upregulated and downregulated, respectively, in the *lncIAPF* overexpressed group compared with the normal group (Figure 5D). These changed genes include two parts: autophagy machinery components and autophagy regulators. Autophagy machinery components contain genes encoding proteins that are involved in autophagic vacuole formation (*ATG4B*, *ATG4C*, *ATG4D*, *ATG9A*, *ATG9B*, *ATG10*, *ATG16 L1*, *ULK1*, *RGS19*, *AMBRA1*, and *GABARAPL2*) and those linking autophagosome to lysosome (*GABARAP*, *LAMP1* and *NPC1*). Autophagy regulators include the co-regulators of autophagy and apoptosis (*IFNG*, *BCL2*, *BCL2L1*, *CDKN1B*, *CDKN2A*, *CXCR4*, *FADD*, *FAS*, *CLN3*, *CASP3*, *IGF1*, *SNCA*, *SQSTM1/P62*, *TGFB1*, *TNF*, and *TNFSF10*) and those responsible for the response to other intracellular signals (*EIF4G1*, *HGS*, *CRPK1*, *CTSS*, *DRAM2* [DNA damage regulated autophagy modulator 2], *PIK3C3*, *RAB24*, *ACTB*, *TMEM74*, and *RPLP0*) (Table 1).

Given that autophagy function is activated by autophagic flux, western blot was used to detect the expression of autophagic flux marker proteins, such as LC3-II:LC3-I and SQSTM1. The expression of SQSTM1 and LC3-II:LC3-I decreased in the normal group. Gain- and loss-of-function studies indicated that LC3-II:LC3-I and SQSTM1 levels were decreased by *lncIAPF* knockdown but increased by *lncIAPF*

overexpression (Figure 5E). Inhibition of *ELAVL1* in autophagy was confirmed by *ELAVL1* effect on autophagic flux. The results identified that LC3-II:LC3-I and SQSTM1 levels were decreased by si-*ELAVL1* but increased by *ELAVL1* overexpression (Figure 5F). The rescue experiment elucidated that interference on *ELAVL1* expression reversed the increasing effect of *lncIAPF* overexpression for autophagic proteins including LC3-II:LC3-I, SQSTM1 (Figure 5G). Therefore, the effect of *lncIAPF* on autophagy depends on *ELAVL1*.

lncIAPF-ELAVL1* complex regulated autophagy through the target genes *EZH2*, *STAT1* and *FOXK1

Potential interactions between *ELAVL1* and other genes were analyzed using GeneMANIA to investigate the effect of *lncIAPF-ELAVL1* axis on autophagy. The results showed that *ELAVL1* directly bound to and regulated the *EZH2* (enhancer of zeste 2 polycomb repressive complex 2 subunit), *STAT1* (signal transducers and activators of transcription 1) and *FOXK1* (forkhead box K1) (Fig. S1C). Emerging evidence has confirmed that both nuclear and cytosolic events can regulate the induction or repression of autophagy [19]. *FOXK1*, *STAT1* and *EZH2* can repress autophagy by controlling the genes associated with autophagy such as *LC3-I*, *LC3-II* and *SQSTM1* via the MTOR pathway in muscle development [20], breast cancer [21] and tumorigenesis [22]. However, this function has not been reported in pulmonary fibrosis. Given their roles in autophagic regulation, *EZH2*, *STAT1* and *FOXK1* were selected for subsequent studies.

First, RNA binding protein immunoprecipitation sequencing (RIP-seq) was performed to identify the target mRNAs to *ELAVL1*. *ELAVL1* RIP-seq data revealed that *ELAVL1* bound to the mRNAs of *EZH2*, *STAT1* and *FOXK1* (Figure 6A, B). RIP-PCR results further confirmed that *ELAVL1* bound to *EZH2*, *STAT1* and *FOXK1* (Figure 6C). RIP-PCR was then used to examine the effects of *lncIAPF* on the binding between *ELAVL1* and its target genes *EZH2*, *STAT1* and *FOXK1* at the mRNA level. The binding degree of *ELAVL1* with *EZH2*, *STAT1* and *FOXK1* was inhibited by *lncIAPF* knockdown but intensified by *lncIAPF* overexpression (Figure 6D). In general, *ELAVL1* can influence mRNA stability. Hence, the mRNA stabilities of *EZH2*, *STAT1* and *FOXK1* were detected by using half-life experiments. The data reflected that the stabilities of *EZH2*, *STAT1* and *FOXK1* were promoted by *lncIAPF* overexpression but reduced by *lncIAPF* knockdown (Figure 6E). Western blot results further confirmed that the protein expression of *EZH2*, *STAT1* and *FOXK1* was decreased by *lncIAPF* knockdown but increased by *lncIAPF* overexpression (Figure 6F). Whether the controlling effect of *lncIAPF* on *EZH2*, *STAT1* and *FOXK1* depends on *ELAVL1* was confirmed by rescue experiments (Figure 6G). *EZH2*, *STAT1* and *FOXK1* expression levels were enhanced by *lncIAPF* overexpression. However, these trends reversed by interference of *ELAVL1* expression, suggesting that the regulating ability of *lncIAPF* for *EZH2*, *STAT1* and *FOXK1* depends on *ELAVL1*. The effects of *EZH2*, *STAT1* and *FOXK1* on fibrotic proteins and autophagic flux were tested by gain- and loss-of-function studies. The results demonstrated that overexpressed *EZH2*, *STAT1* and *FOXK1*

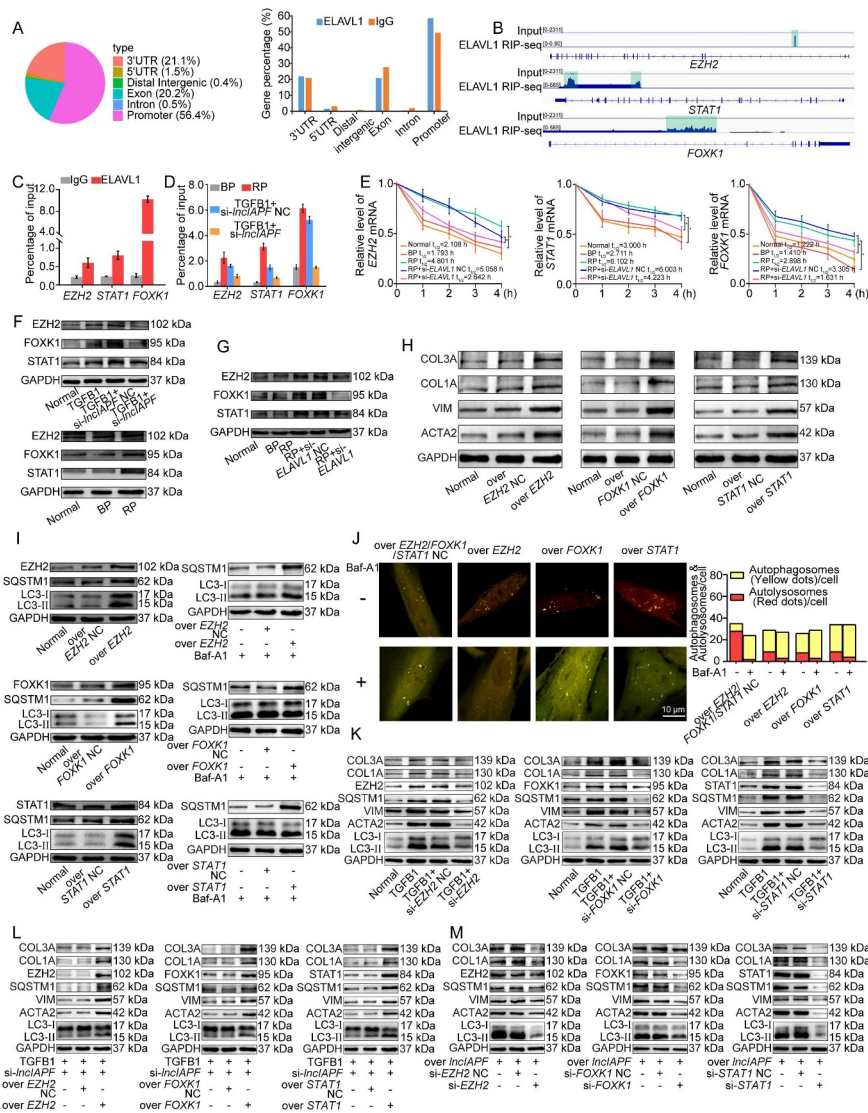


Figure 6. *Lnc1APF*-*ELAVL1* complex regulated autophagy through the target genes *EZH2*, *STAT1* and *FOXK1*. (A) *ELAVL1* RIP-seq peaks were categorized according to the distribution on different genomic elements of *ELAVL1* and compared with the genomic background. (B) Representative *ELAVL1* RIP-seq peaks were shown as track signals in an integrative genomic viewer. Peak area is highlighted in light green. The mRNAs of *EZH2*, *STAT1* and *FOXK1* bound to *ELAVL1*. (C) RIP-PCR results confirmed that the mRNAs of *EZH2*, *STAT1* and *FOXK1* bound to *ELAVL1*. (D) RIP-PCR results validated that *Inc1APF* knockdown repressed the binding amount of *ELAVL1* with *EZH2*, *STAT1* and *FOXK1*, whereas *Inc1APF* overexpression increased the binding amount. (E) Half-life experiments detected the mRNAs stabilities of *EZH2*, *STAT1* and *FOXK1*. *Lnc1APF* overexpression promoted their stabilities and *si-ELAVL1* reduced the growing trend of stabilities. (F) Western blot results manifested that *Inc1APF* knockdown expression decreased *EZH2*, *STAT1* and *FOXK1* levels, *Inc1APF* overexpression increased their expression trends. (G) Rescue experiments indicated that *Inc1APF* overexpression increased *EZH2*, *STAT1* and *FOXK1* levels. Interference of *ELAVL1* expression induced their expression trends reversed. (H) Overexpressed *EZH2*, *STAT1* and *FOXK1* promoted the expression of *ACTA2*, *COL1A*, *COL3A* and *VIM*. (I) Effects of the target genes *EZH2*, *STAT1* and *FOXK1* on autophagic flux. Overexpression of *EZH2*, *STAT1* and *FOXK1* promoted *SQSTM1* and *LC3-II:LC3-I* expression. (J) Red fluorescence was weakened in the groups of *EZH2*, *STAT1* and *FOXK1* overexpression, indicating that their overexpression reduced the autophagosome-lysosome fusion. Baf-A1 worked the same as *EZH2*, *STAT1* and *FOXK1*. (K) Knockdown *EZH2*, *STAT1* and *FOXK1* inhibited the expression of fibrotic proteins and promoted autophagic flux. (L) The rescue experiment elucidated that overexpressed *EZH2*, *STAT1* and *FOXK1* reversed the downward trend of fibrotic and autophagic proteins caused by *si-Inc1APF*. (M) Knockdown *EZH2*, *STAT1* and *FOXK1* reversed the downward trend of fibrotic and autophagic proteins caused by overexpressed *Inc1APF*. Each bar represents the mean \pm SD; $n = 6$; $p < 0.05$.

promoted the expression of fibrotic proteins and inhibited autophagic flux (Figure 6H,I). Also, Baf-A1 was added to confirm blockade of the fusion between autophagosome and lysosome in overexpressed *EZH2*, *STAT1* and *FOXK1* groups, not autophagosome formation. Overexpressed *EZH2*, *STAT1* and *FOXK1* inhibited the fusion of autophagosome and lysosome (Figure 6J). Knockdown *EZH2*, *STAT1* and *FOXK1* inhibited the expression of fibrotic proteins and promoted autophagic flux (Figure 6K). The rescue experiments elucidated that overexpressed *EZH2*, *STAT1* and *FOXK1* reversed the downward trend of fibrotic and autophagic proteins

caused by *si-Inc1APF* (Figure 6L), whereas knockdown of *EZH2*, *STAT1* and *FOXK1* reversed the upward trend of these proteins caused by overexpressed *Inc1APF* (Figure 6M).

The effects of *EZH2*, *STAT1* and *FOXK1* on autophagy were further studied by using human autophagy RT² profiler PCR arrays (Figure 7A). The overexpression of *EZH2*, *STAT1* and *FOXK1* co-regulated 30 upregulated and 13 downregulated ATGs (Table 2–4). Among these genes, 21 upregulated ATGs, namely, *ATG4B*, *ATG4D*, *ATG9B*, *ATG9A*, *ATG10*, *ATG16L1*, *ULK1*, *RGS19*, *AMBRA1*, *LAMP1*, *NPC1*, *BCL2L1*, *CDKN1B*, *FADD*, *CLN3*, *IGF1*, *SQSTM1*, *TGFβ1*, *TNFSF10*,

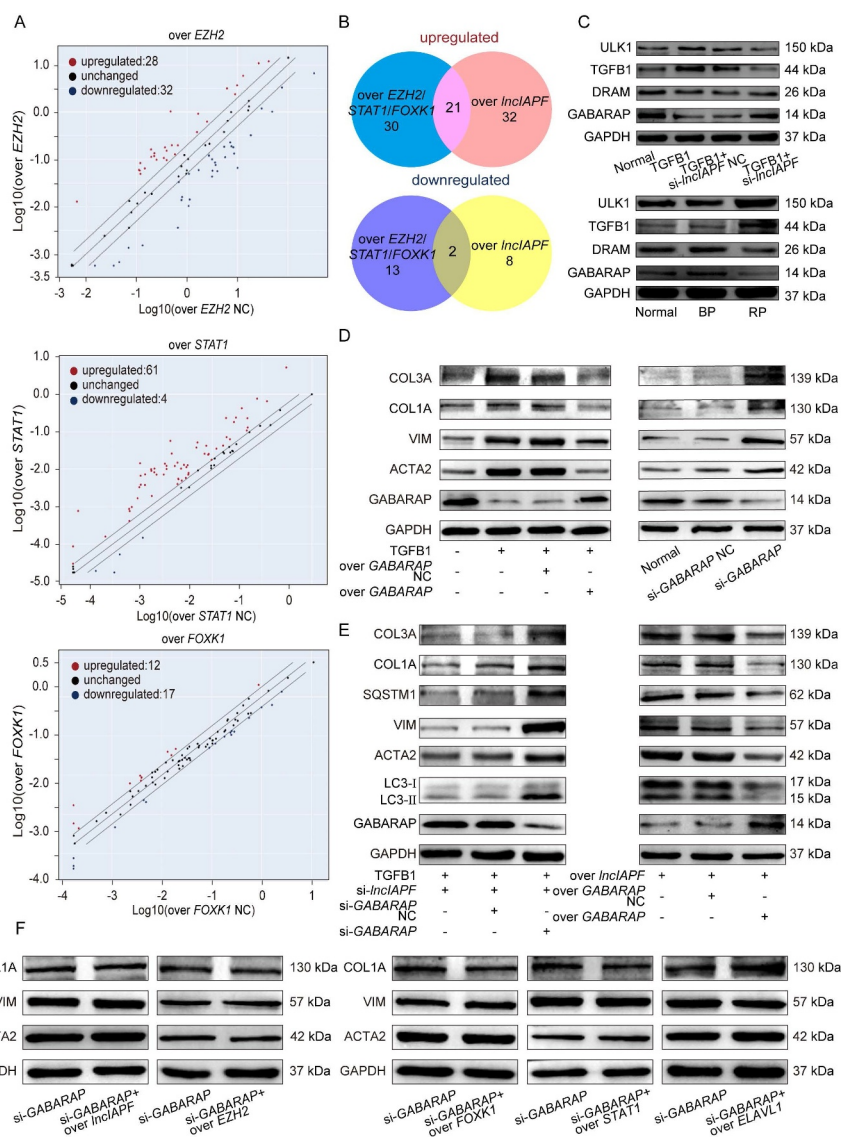


Figure 7. Coregulation of overexpressed *EZH2*, *STAT1* and *FOXK1* on ATGs and fibrotic proteins. (A) Effects of overexpressed *EZH2*, *STAT1* and *FOXK1* on autophagy were tested by human autophagy RT² profiler PCR array. (B) Venn diagrams showed the number of changed ATGs co-regulated by overexpressed *EZH2*, *STAT1*, *FOXK1* and *lncIAPF*. (C) Western blot showed that DRAM2 and GABARAP levels decreased by overexpressed *lncIAPF* and increased by knockdown *lncIAPF*. ULK1 and TGFB1 levels increased by overexpressed *lncIAPF* and decreased by knockdown *lncIAPF*. (D) Overexpressed GABARAP reduced fibrotic protein expression and knockdown GABARAP promoted their expression. (E) The rescue experiments elucidated that si-GABARAP reversed the decreasing trend of fibrosis and the increasing trend of autophagic flux caused by *lncIAPF* knockdown. Overexpressed GABARAP reversed the increasing trend of fibrosis and the decreasing trend of autophagic flux caused by overexpressed *lncIAPF*. (F) Western blot demonstrated that the pro-fibrotic function of *EZH2*, *STAT1*, *FOXK1* was not strengthened.

HGS, and *ACTB*, overlapped with those regulated by *lncIAPF* overexpression. Two downregulated ATGs, namely, *DRAM2* and *GABARAP* (GABA type A receptor-associated protein), overlapped with those regulated by *lncIAPF* overexpression (Figure 7B). Western blot analysis further confirmed that *DRAM2* and *GABARAP* levels were increased by *lncIAPF* knockdown but decreased by *lncIAPF* overexpression. ULK1 (unc-51-like autophagy activating kinase 1) and TGFB1 were decreased by *lncIAPF* knockdown but increased by *lncIAPF* overexpression (Figure 7C). *DRAM2* and *GABARAP* contribute to autophagy via autophagosome-lysosome fusion [23,24]. ULK1 mainly help for the early stage of autophagy. This finding supports the conclusion that *lncIAPF* overexpression inhibits autophagy by blocking autophagosome

fusion with lysosome. Gain- and loss-of-function studies were performed to measure the effect of *GABARAP* on fibrosis. Overexpressed *GABARAP* reduced fibrotic protein expression and knockdown *GABARAP* promoted their expression (Figure 7D). The rescue experiments elucidated that si-GABARAP reversed the decreasing trend of fibrosis and the increasing trend of autophagic flux caused by *lncIAPF* knockdown. Overexpressed *GABARAP* reversed the increasing trend of fibrosis and the decreasing trend of autophagic flux caused by overexpressed *lncIAPF* (Figure 7E). To further clarify the correlation between fibrosis and autophagy, si-GABARAP packaged into the adenovirus vector was transfected into MRC-5 cell. Western blot demonstrated that overexpressed *EZH2*, *STAT1*, *FOXK1* and

Table 4. The altered ATGs in overexpressed *FOXK1* group.

Gene Symbol	Fold Regulation	Gene Symbol	Fold Regulation
<i>ATG10</i>	2.67	<i>CTSS</i>	-2.36
<i>ATG16L1</i>	3.02	<i>CXCR4</i>	-4.21
<i>CDKN1B</i>	2.46	<i>DRAM2</i>	-1.87
<i>DAPK1</i>	3.38	<i>ESR1</i>	-1.89
<i>GAA</i>	2.19	<i>GABARAP</i>	-1.84
<i>HGS</i>	2.01	<i>HSP90AA1</i>	-2.60
<i>INS</i>	9.93	<i>HSPA8</i>	-1.85
<i>RGS19</i>	2.22	<i>IRGM</i>	-2.50
<i>TGFB1</i>	2.07	<i>PIK3CG</i>	-3.58
<i>TNFSF10</i>	1.89	<i>PRKAA1</i>	-1.87
<i>ULK1</i>	2.63	<i>RB1</i>	-1.85
<i>ACTB</i>	2.33	<i>TGM2</i>	-2.31
<i>ATG3</i>	-2.20	<i>TNF</i>	-2.27
<i>BID</i>	-1.80	<i>WIP1</i>	-1.96
<i>BNIP3</i>	-1.93		

The positive number indicates upregulation and the negative number indicates downregulation.

ELAVL1 promoted fibrotic proteins expression (Figure 7F). These results reflected that the regulatory signals of *lncIAPF* on autophagy are mainly exhibited through *EZH2*, *STAT1* and *FOXK1*.

***lncIAPF* as a potential therapeutic target for pulmonary fibrosis**

Animal experiments and clinical studies were performed to evaluate the potential of *lncIAPF* as a therapeutic target. Given that *lncIAPF* was screened from human fibroblast, it has a relatively low degree of homology to that in mice. Therefore, we first test whether overexpressed humanized *lncIAPF* was effective in mice to validate the mouse model is relevant to the proposed mechanism. In mouse fibroblast L929 cells, qRT-PCR results indicated that overexpressed *lncIAPF* promoted *lncIAPF* expression (Fig. S2A). Western blot results illustrated that overexpressed *lncIAPF* promoted fibrogenesis and inhibited autophagy (Fig. S2B,C). In BLM-treated mice model, bleomycin also promoted these proteins expression (Fig. S2D). The findings corroborated the human fibroblast results, which suggest that the mouse model is relevant to the proposed mechanism. Hence, we can use mice model to further confirm the proposed mechanism.

Due to poor homology, perhaps *lncIAPF* interference does not work effectively in mice model. According to the similar study [25], overexpressed *lncIAPF* was selected for mice experiments. Overexpressed *lncIAPF* was packaged into the adenovirus vector marked with green fluorescent protein and sprayed into the mouse lung from the trachea (Figure 8A). The efficiency of overexpressed *lncIAPF* was detected by qRT-PCR. The data proved the high expression of *lncIAPF* in the overexpressed *lncIAPF*-treated mice, indicating that the overexpressed *lncIAPF* adenovirus vector is highly efficacious (Figure 8B). Lung-function assessment revealed that *lncIAPF* overexpression affected the forced vital capacity (FVC) of mice (Figure 8C). H&E and Masson staining results presented massive collagen deposits, fibrosis lesions, and distorted lung architecture in the overexpressed *lncIAPF* group compared with those in the sham group (Figure 8D, E). Western blot

results further confirmed that *lncIAPF* overexpression increased the levels of fibrotic and differentiation-related proteins including COL1A, VIM, ACTA2, FAP, S100A4 and decreased that of epithelial marker CDH1/E-cadherin (Figure 8F). Meanwhile, the expression of enhanced autophagic proteins including SQSTM1, LC3II:LC3I, ELAVL1, EZH2, STAT1 and FOXK1 (Figure 8G) was increased, suggesting that *lncIAPF* promotes pulmonary fibrosis by blocking autophagy in vivo.

To improve the convincing mechanism and overcome the low degree homology of *lncIAPF* in mice, we synthesized si-*ELAVL1* packaged into the adenovirus vector to spray into the mouse lung. Body weight monitoring revealed that BLM-treated mice lost substantial body mass compared with sham mice. However, si-*ELAVL1* effectively blocked this loss compared with the control group (Figure 8H). The results of MicroCT imaging system for small animal demonstrated that fibrosis changes occurred in both lungs in BLM group, and the degree of fibrosis was significantly reduced in si-*ELAVL1* group (Figure 8I). Lung function assessment demonstrated that the FVC was improved in si-*ELAVL1* group (Figure 8J). H&E and Masson images revealed that excess collagen was deposited and the alveolar wall became thicker in BLM group, and si-*ELAVL1* attenuated collagen deposition (Figure 8K). Western blot results further confirmed that the levels of fibrotic, differentiation-related and autophagic proteins reduced in si-*ELAVL1* group (Figure 8L). The findings indicated that si-*ELAVL1* had significant therapeutic effect. Meanwhile, the findings also suggested that *lncIAPF* promotes pulmonary fibrosis by blocking autophagy in vivo through the proposed mechanism.

Finally, to assess the clinical application value, *lncIAPF* and the related gene expression were explored in patients with IPF. The characteristics and physiologies of patients with IPF were shown in Table 5. *lncIAPF* was highly upregulated in the blood collected from patients with IPF (Figure 9A). The receiver operating characteristic curve (ROC) between *lncIAPF* and FVC showed that the sensitivity and specificity values are 87.5% and 75.0% in IPF patients, respectively. The area under the ROC curve was 0.879 (Figure 9B). ROC curve between *lncIAPF* and DLco showed that the sensitivity and specificity values are 42.9% and 78.6%, respectively. The area under the ROC curve was 0.579 (Figure 9C). ROC curve between *lncIAPF* and PaO₂ showed that the sensitivity and specificity values are 92.9% and 92.0%, respectively. The area under the ROC curve was 0.949 (Figure 9D). ROC curve between *lncIAPF* and PaCO₂ showed that the sensitivity and specificity values are 50.0% and 87.5%, respectively. The area under the ROC curve was 0.520 (Figure 9E). Immunofluorescence staining of lung tissues revealed that LC3 and SQSTM1 increased in the patients with IPF. These findings imply that autophagy was blocked. The levels of ELAVL1 and its target genes EZH2, STAT1 and FOXK1 also increased in the patients with IPF (Figure 9F). These clinical findings corroborated the in vivo and in vitro results, indicating that interference in *lncIAPF* expression may offer a novel biomarker or therapeutic approach against IPF.

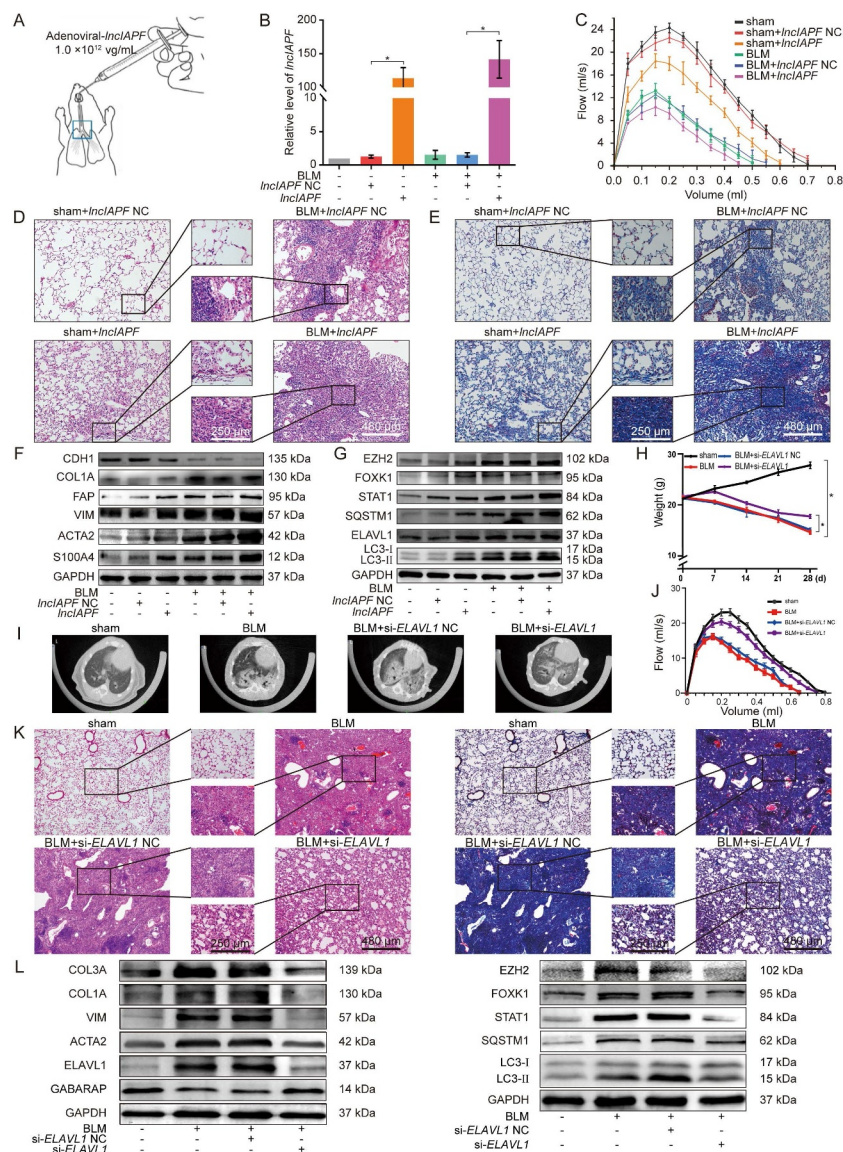


Figure 8. Assessment of *IncIAPF* as a potential therapeutic target in mice. (A) Adenoviral *IncIAPF* was inhaled by mice through spraying. (B) qRT-PCR results clarified that overexpressed *IncIAPF* was highly expressed in the mouse model, indicating that the adenoviral vector was constructed successfully. (C) FVC results described that overexpressed *IncIAPF* affected the lung function of mice compared with that in the control group. (D) Histological images of lung paraffin sections stained with H&E manifested that the alveolar walls were thickened and filled with pink collagen in the overexpressed *IncIAPF* group. (E) Collagen deposition increased in the lung tissue of overexpressed *IncIAPF*-treated mice detected by Masson's trichrome staining. (F) Fibrotic proteins such as COL1A, VIM and ACTA2 increased in the overexpressed *IncIAPF*-treated mice. The levels of differentiation-related proteins FAP and S100A4 also increased, but that of the epithelial marker CDH1 decreased. (G) Autophagy proteins SQSTM1 and LC3II:LC3I had increased levels in overexpressed *IncIAPF*-treated mice. (H) Body weight monitoring revealed that BLM-treated mice lost substantial body mass compared with sham mice. si-*ELAVL1* effectively blocked this loss compared with the control group. (I) MicroCT imaging system for small animal demonstrated that fibrosis changes occurred in both lungs in BLM group, and the degree of fibrosis was significantly reduced in si-*ELAVL1* group. (J) Lung function assessment demonstrated that the FVC was improved in si-*ELAVL1* group. (K) H&E and Masson images revealed that excess collagen was deposited and the alveolar wall became thicker in BLM group, and si-*ELAVL1* attenuated collagen deposition. (L) Western blot results showed that the levels of fibrotic, differentiation-related proteins and autophagic proteins reduced in si-*ELAVL1* group. Each bar represents the mean \pm SD; n = 6; *p < 0.05.

Discussion

lncRNAs are crucial to epigenetic regulation and participate in the pathogenesis of various diseases [26,27]. Their location determines their regulatory mechanisms. Nuclear lncRNA mainly regulates chromatin, transcription, or alternative splicing; and cytoplasmic lncRNA mainly affects mRNA stability, protein translation, or posttranslational modification. For example, the nuclear lncRNA *MALAT1* suppresses antiviral innate responses by directly binding to TARDBP/TDP43 (TAR DNA binding protein) in the nucleus and prevents

the activation of TARDBP43 by blocking the activated CASP3 (caspase 3)-mediated TARDBP43 cleavage to TARDBP35. The cleaved TARDBP35 increases the nuclear IRF3 protein level by binding and degrading *Rbck1* pre-mRNA to prevent IRF3 proteasomal degradation upon viral infection, thus selectively promoting antiviral IFN-I production [28]. The cytoplasmic lncRNA *H19-DMD* (dystrophin) interactions inhibit E3-ligase-dependent polyubiquitination at Lys 3584 in Duchenne muscular dystrophy, thus preventing protein degradation [29]. The pan-cancer lncRNA *MILIP*

Table 5. Characteristics and physiologies of IPF patients and the normal.

Characteristic	Normal	IPF patients	P value
Number	20	20	/
Age (years)	69.93 ± 7.5	71.75 ± 8.70	/
Gender (Male/Female)	15/5	13/7	/
FVC (% of predicted)	89.7 ± 3.7	64.09 ± 9.39	<0.01
DL _{CO} (% of predicted)	88.8 ± 3.3	54.12 ± 8.92	<0.01
PaO ₂ (mmHg)	85.6 ± 2.6	59.0 ± 3.46	<0.01
PaCO ₂ (mmHg)	35.2 ± 5.7	43.99 ± 6.61	<0.01
Smoking History (n)	12	12	/

Data are depicted as means ± SD. FVC, forced vital capacity; DL_{CO}, diffusing capacity for carbon monoxide; smoking history denotes subjects with >5 pack-years of cigarette smoking.

mainly located in cytoplasm is critical for cancer cell survival, division, and tumorigenicity. Yu et al. reported that MYC/c-Myc can alternatively inactivate TP53/p53 through the

lncRNA *MILIP*, which restrains TP53 SUMOylation by suppressing the SUMO E3 ligase TRIML2 (tripartite motif family like 2) and consequently facilitates TP53 polyubiquitination and turnover [30]. In the present study, *lncIAPF* was found in the nucleus and cytoplasm and functioned as a pro-fibrotic factor to facilitate pulmonary fibrosis by promoting fibroblast-to-myofibroblast differentiation and myofibroblast proliferation and migration. Mechanistic studies revealed that H3K27ac and ATF3 bind to the chromatin open region of *lncIAPF* promoter and thereby enhance *lncIAPF* transcription. The highly expressed *lncIAPF* forms an RNA-protein complex with ELAVL1 to inhibit autophagosome fusion with lysosome by controlling the stability of the target genes *EZH2*, *STAT1* and *FOXK1* (Figure 10). Moreover, the clinical value of *lncIAPF* as a therapeutic target for IPF was verified.

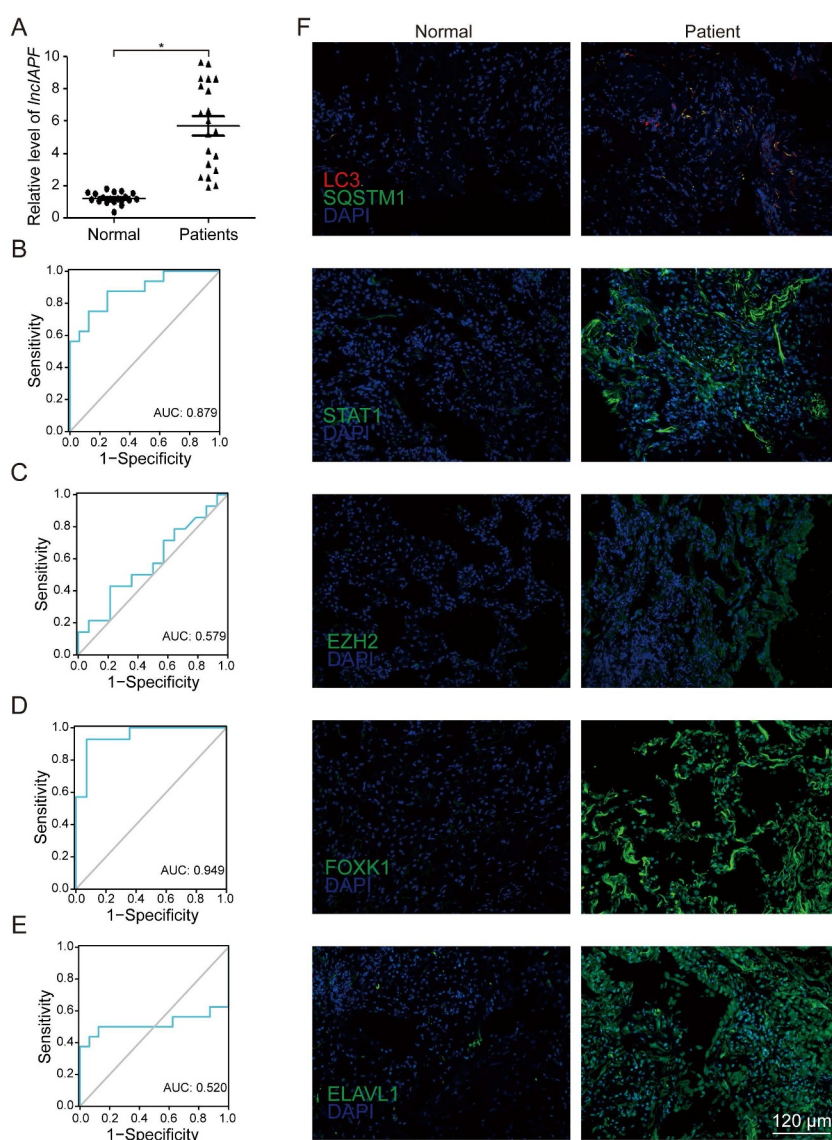


Figure 9. Assessment of *lncIAPF* value in IPF patients. (A) Expression levels of *lncIAPF* increased in 20 patients with IPF as detected by qRT-PCR. (B) ROC curve between *lncIAPF* and FVC showed that the sensitivity and specificity values are 87.5% and 75.0% in IPF patients, respectively. The area under the ROC curve was 0.879. Confidence interval (CI): 0.762–0.996. (C) ROC curve between *lncIAPF* and DL_{CO} showed that the sensitivity and specificity values are 42.9% and 78.6% in IPF patients, respectively. The area under the ROC curve was 0.579. Confidence interval (CI): 0.360–0.798. (D) ROC curve between *lncIAPF* and PaO₂ showed that the sensitivity and specificity values are 92.9% and 92.0% in IPF patients, respectively. The area under the ROC curve was 0.949. Confidence interval (CI): 0.872–1.000. (E) ROC curve between *lncIAPF* and PaCO₂ showed that the sensitivity and specificity values are 50.0% and 87.5% in IPF patients, respectively. The area under the ROC curve was 0.520. Confidence interval (CI): 0.281–0.758. (F) Red fluorescence of autophagosome and the expression of SQSTM1, ELAVL1, EZH2, STAT1, and FOXK1 all increased in IPF patients compared with those in the normal group. Blue fluorescence indicated DAPI. The images are representative of six independent experiments.

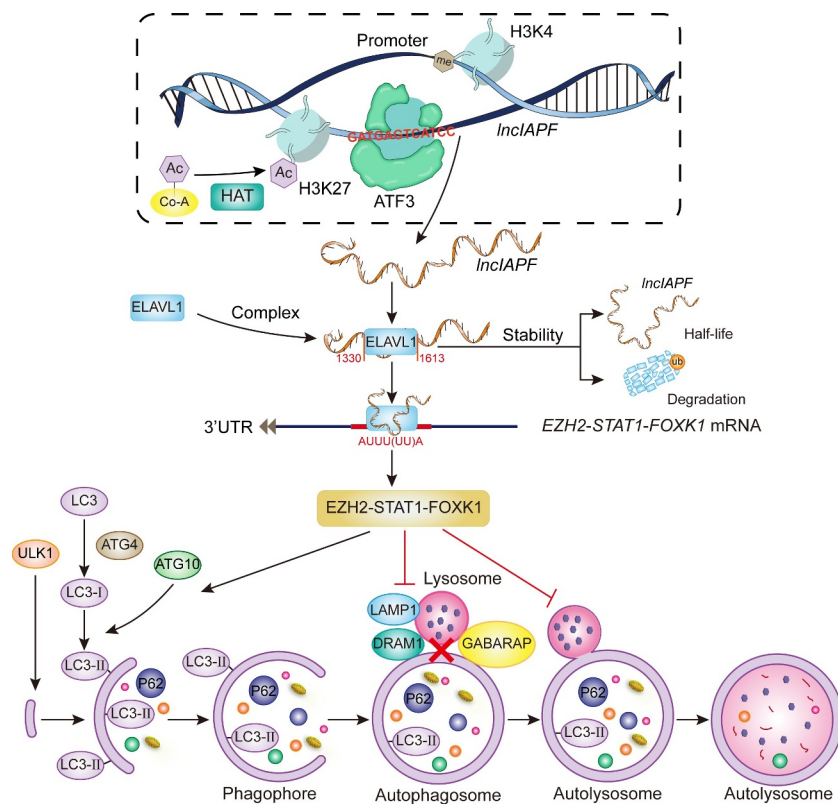


Figure 10. Mechanism of *lncIAPF* functioning as a pro-fibrotic factor that promotes pulmonary fibrosis.

Many factors can cause lncRNA expression changes. For example, 8p12 loci loss of *LINCTSLNC8* reduces *LINCTSLNC8* expression, leading to hepatocellular carcinoma malignancies [31]. H3K27 acetylation-activated *lncCCAT1* affects cell proliferation and migration by regulating *SPRY4* and *HOXB13* expression in esophageal squamous cell carcinoma [32]. The transcription factor TP63 binds to the super enhancer at the *LINC01503* locus and activates its transcription, leading to squamous cell carcinoma cell proliferation, migration, invasion, and xenograft tumor growth [33]. However, no direct factors that induce lncRNA change in pulmonary fibrosis have been reported. Here, H3K27ac was found to activate the chromosome region of *lncIAPF* promoter opening during fibrogenesis. As a regulator, the transcription factor ATF3 bound to the *lncIAPF* promoter and enhanced the *lncIAPF* expression.

lncRNAs are closely associated with the development of pulmonary fibrosis, particularly by acting as pro- or anti-fibrotic factors in several process such as alveolar epithelial cell injury [34], fibroblast-to-myofibroblast transition, extracellular-matrix deposition [35], and macrophage activation [36]. lncRNA participation in fibroblast differentiation into myofibroblasts is one of the research focus on pulmonary fibrogenesis. For example, lncRNA *DNM3OS* contributes to fibroblast differentiation into myofibroblast function as a reservoir of three miRNAs, namely, *MIR199A-5p*, *MIR199A-3p* and *MIR214-3p*, through the TGF β signaling pathway [37,38]. *lncPFAR* enhances lung

fibroblast activation by sponging *MIR138* to regulate the YAP1-Twist axis [39]. *lncFENDRR* [40], *lncCDKN2B-AS1* [41] and *lncPFAL* [42] can accelerate lung fibrosis by accelerating fibroblast differentiation into myofibroblast. Various kinds of ncRNAs, such as lncRNA, miRNA, circRNA and mRNA, can even form a fine regulatory network to control fibroblast differentiation into myofibroblast. *lnc865*, *lnc556*, *circ949*, *circ057*, *Mir29b-2-5p* and *STAT3* are typical examples. Among which, *lnc865* and *lnc556* can crosstalk with *circ949* and *circ057* by sponging *Mir29b-2-5p* to target *STAT3* translocation. After phosphorylation, p-*STAT3* as a transcription factor can be transported into the nucleus from the cytoplasm and activate gene expression [43]. However, the lncRNA regulation of fibroblast-to-myofibroblast differentiation through the autophagy signal pathway in pulmonary fibrosis is poorly investigated. Our data reported that the highly upregulated *lncIAPF* promotes fibroblast-to-myofibroblast differentiation and myofibroblast proliferation and migration by blocking autophagy in pulmonary fibrosis.

Autophagy is a type II programmed cell death in which cellular components are sequestered in an autophagosome, which then fuses with a lysosome to degrade those contents. Dysregulated autophagy has implications in health and diseases [44,45]. In general, autophagy is a protective mechanism in the lung of patients with IPF [46]. Autophagy deficiency in macrophages exacerbates inflammation and fibrosis following silica exposure [47] and bleomycin

challenge [48]. Targeting autophagy in IPF, including the use of IL17A (interleukin 17A) neutralizing antibodies [49], *Mir449a* [50], or PDGFRB (platelet derived growth factor receptor beta) inhibitors, may offer a therapeutic potential [51]. Recently, more and more lncRNAs are revealed to be involved in the regulation of autophagy. In-vitro and in-vivo experiments uncover that lncRNA *EIF3J-DT* activates autophagy and induced drug resistance in gastric cancer cells by targeting *ATG14* [52]. LncRNA *SNHG11* aggravates oncogenic autophagy to facilitate cell proliferation, stemness, migration, invasion and epithelial-to-mesenchymal transition in gastric cancer [53]. LncRNA *BCYRN1*-induced autophagy enhances asparaginase resistance in extranodal NK/T-cell lymphoma [54]. In pulmonary fibrosis, Ni's group found that silica-induced pulmonary fibrosis is facilitated by *lncHOTAIR* through the sponging of *MIR326* and attenuated by the increased *MIR326* expression through the promotion of the autophagy activity of fibroblasts by targeting PTBP1 (polypyrimidine tract binding protein 1). However, the direct regulation between *lncHOTAIR* and autophagy has not yet been clarified [55]. The present study revealed that *lncIAPF* directly controls autophagy by blocking autophagosome fusion with lysosome depending on ELAVL1 in pulmonary fibrosis; knockin *lncIAPF* blocked autophagy, whereas *lncIAPF* knockdown enhanced this process. We reasoned that *lncIAPF* binds to ELAVL1 protein and blocks ELAVL1 susceptibility to ubiquitination and degradation, thereby increasing the levels of ELAVL1 and its target autophagy-related mRNAs such as *EZH2*, *STAT1* and *FOXK1* that are negatively associated with autophagy. These changes prevent autophagy.

As an RNA-binding protein, ELAVL1 participates in disease occurrence and progression by binding to lncRNAs. The macrophage-specific *lncMAARS* regulates apoptosis and atherosclerosis by tethering ELAVL1 in the nucleus [56]. *lncOCC-1* suppresses cell growth by destabilizing ELAVL1 protein in colorectal cancer [16]. However, ELAVL1 binding to lncRNA in pulmonary fibrosis has not yet been reported. In this work, *lncIAPF* bound to ELAVL1 in pulmonary fibrosis and that the *lncIAPF*-ELAVL1 complex regulated autophagy flux through the target genes *EZH2*, *STAT1* and *FOXK1*. *EZH2* functions as a histone methyltransferase by catalyzing histone methylation at H3 Lys27. *STAT1* and *FOXK1* function as transcription factors and play important roles in cell growth, differentiation and death [57–59]. As cytosolic genes, these three genes can control autophagy [19–22]; however, this function has not been reported in pulmonary fibrosis. The findings indicated that together with the *lncIAPF*-ELAVL1 complex, these three genes negatively regulate autophagy in pulmonary fibrosis.

Although lncRNAs have been found in humans, only a small number of lncRNAs have been functionally characterized in pulmonary fibrosis, and most of their mechanisms are largely unknown. Our observations confirmed that *lncIAPF* overexpression accelerates fibroblast-to-myofibroblast differentiation by blocking autophagy in pulmonary fibrosis, and this effect is dependent on ELAVL1. This finding provides a novel treatment strategy related to autophagy for IPF.

Materials and methods

IPF patients

IPF patients were diagnosed in accordance with the American Thoracic Society and European Respiratory Society criteria for IPF, and age-matched healthy controls at Binzhou Medical University Hospital were included. All patients provided written informed consent, and ethical consent was obtained from the Committee of Binzhou Medical University.

Animal treatment

Experiments on the studied animals were approved by the Committee on the Ethics of Animal Experiments of Binzhou Medical University. Eight-week-old C57BL/6 mice were obtained from the Model Animal Research Center of Nanjing University (Nanjing, China). All mice were bred and maintained in a 12 h light/dark cycle and allowed free access to food and water. The mice were divided into different groups (10 mice in each group) according to the experimental requirements. The BLM-treated mouse was administered 5 mg/kg bleomycin, which was sprayed into the lungs using a Penn-Century MicroSprayer (Penn-Century Inc., Wyndmoor, PA, USA). The experimental mice were administered 1.0×10^{12} vg/mL adenoviral-*lncIAPF/NC* or adenoviral-si-*ELAVL1/NC*, which was also sprayed into the lungs using a Penn-Century MicroSprayer. The sham group only received the same amount of normal saline as the control group. Lung tissues were harvested on the 28th day following treatment.

Cell model

Human fetal lung fibroblast (MRC-5 cell line) and mouse fibroblast (L929 cell line) were obtained from American Type Culture Collection (CCL-171™ and CCL-1™) and cultured at 37°C in an atmosphere containing 5% CO₂ and in advanced minimum essential medium (MEM; Gibco, 11,090,081), supplemented with 10% fetal bovine serum. The

Table 6. The item number and brand of the antibody.

Antibody Name	Item number	Brand of the antibody
GAPDH	AF7021	Affinity
ACTA2/a-SMA	AF1032	Affinity
VIM	AF7013	Affinity
COL1A	AF7001	Affinity
COL3A	AF0136	Affinity
FOXK1	12,025	Cell Signaling Technology
EZH2	49055	Cell Signaling Technology
STAT1	91725	Cell Signaling Technology
ELAVL1	12,582	Cell Signaling Technology
SQSTM1/p62	AF5384	Affinity
LC3-I/II	Ab128025	Abcam
TGFB1	Ab215715	Abcam
GABARAP	18723-1-AP	Proteintech
ULK1	AF4387	Affinity
DRAM	Ab208160	Abcam
FSP1	20,886-1-AP	Proteintech
FAP	Ab207178	Abcam
TUBB/β-Tubulin	DF7967	Affinity
Histone H3	AF0863	Affinity
CDH1/E-cadherin	AF0131	Affinity
ATF3	18,665	Cell Signaling Technology

cells were treated with 5 ng/mL TGF β 1 (Gibco, PHG9202) for different times according to the requirement of experiments.

Western-blot Western blot were performed using standard protocols established in our laboratory, specific steps were referred to published articles [11]. The item number and brand of the antibody were listed in Table 6.

ATAC-seq

Fifty μ L pre-cooled RSB (containing 0.1% NP40 [Thermo Scientific, 85,124], 0.1% Tween-20 [Thermo Scientific, 28,320], 0.01% digitalis saponin [MedChemExpress, HY-N4000]) was added to 5×10^4 living cells, which were incubated on ice for 3 min. Then, 1 mL pre-cooled RSB only contained 0.1% Tween-20 was added and centrifuged at 500 g for 5 min. The supernatant was removed. The precipitate was resuspended with 50 μ L transposition mix (TD, 2 \times reaction buffer from Nextera kit [Illumina, FC-121-1030], 25 μ L; TDE1, Nextera Tn5 Transposase from Nextera kit, 2.5 μ L; and nuclease-free H $_2$ O 22.5 μ L; total volume 50 μ L), and placed into a mixometer (Youning, Hangzhou China) at 177 \times g for 30 min. The DNA was first purified with Qiagen MinElute PCR Purification Kit (QIAGEN, 28,004), and was further purified with Zymo DNA Clean and Concentrator-5 Kit (ZYMO RESEARCH, D4004). Then PCR was performed in a 50 μ L final volume as follows: 7 cycles of 98 $^\circ$ C for 3 min, 98 $^\circ$ C for 15s, and 63 $^\circ$ C for 30s, finally, 72 $^\circ$ C for 30s, 72 $^\circ$ C for 5 min. The PCR product was sequenced by illuminaHiSeq/NextSeq platform. Subsequently, the data was analyzed using unique mapped reads.

Real-time cellular proliferation and migration analyses

Cells (5×10^4) were cultured in E-plate (proliferation plate; Agilent, 5,469,830,001) and CIM-plate (migration plate; Agilent, 05665817001), respectively, in an RTCA DPlus instrument system. The proliferation and migration curves were automatically recorded by the system. Cell index representing the amount of proliferating or migrating cells was calculated by using RTCA from ACEA Biosciences (ACEA Biosciences, China), as previously described in a study [11].

Wound healing assay

Cells (5×10^5) were seeded in a 96-well plate and incubated in an incubator. After overnight incubation, the cells were wounded with cell scratcher, washed with PBS (SparkJade, CR0013-500ML), replaced with complete medium culture, and placed in IncuCyte S3 live-cell analysis system (Essen BioScience, USA) for real-time dynamic observation. Images were taken on IncuCyte S3 software.

RNA affinity-isolation assay

RNA affinity-isolation assay was carried out as previously described [11]. Briefly, *InclAPF* transcripts were transcribed using T7 and SP6 RNA polymerase in vitro, then by using the RNeasy Plus Mini Kit (QIAGEN, 74,134) and treated with TURBO DNase I. Purified RNAs were biotin-labeled using

Biotin RNA Labeling Mix (Roche Diagnostics, 11,685,597,910). The biotinylated *InclAPF* and its antisense RNAs were mixed and incubated with cell lysates. Then, avidin magnetic beads were added to each binding reaction, and the mixtures were incubated. The binding proteins were separated by SDS-PAGE, visualized by silver staining and identified by regular liquid chromatography-mass spectrometry and western blot analysis.

Human autophagy RT² profiler PCR array

Cells were collected and extracted RNA. Complementary DNA synthesis was performed according to the RT² First Strand kit (QIAGEN, 330,404). After cDNA obtainment, the PCR reaction was carried out in a 25 μ L final volume using 40 ng cDNA as follows: initial denaturation at 95 $^\circ$ C for 10 min, followed by 40 cycles of 95 $^\circ$ C for 15s, 55 $^\circ$ C for 35s and 72 $^\circ$ C for 30 min.

RNA FISH observation

RNA FISH was performed with the FISH kit according to the manufacturer's protocol (Ribo Bio Technology, C10910). Cells were seeded in a 24-well plate. When the cell density reached 50–60%, the medium was discarded and 4% paraformaldehyde was added. After washing with PBS, 500 μ L of pre-cooled permeate solution was added into cell samples for 3 min. Then permeate solution was washed away with PBS, 200 μ L pre-hybridization buffer was added to each well and incubated for 30 min. Subsequently, 100 μ L 20 μ M *InclAPF*, *RNA18S* and *RNU6* FISH Probe Mix were added to each well and incubated overnight. Cells were washed with SSC (Solarbio, S1030) and PBS solution, and stained with DAPI staining solution for 10 min. Finally, the images were observed with a confocal microscope.

RIP analysis

RIP assays were performed using an EZ-Magna RIP[™] RNA-binding protein immunoprecipitation kit (Millipore, 17–701) according to the manufacturer's instructions. Cells at approximately 90% confluence was lysed using complete RIP lysis buffer containing RNase inhibitor and protease inhibitor and then 100 μ L of whole cell extract was incubated with RIP buffer containing magnetic beads conjugated to specific antibody (Cell Signaling Technology, 12,582). The nonspecific control was normal rabbit anti-IgG antibody (Cell Signaling Technology, 2729). Purified RNA was subjected to qRT-PCR analysis.

ChIP-PCR

ChIP-PCR was performed following the SimpleChIP[®] Plus Sonication Chromatin IP Kit protocol (Cell Signaling Technology, 56,383). Briefly, cells were crosslinked with 1% formaldehyde in culture medium for 10 min at room temperature, and chromatin from lysed nuclei was sheared to 200–600 bp fragments. Chromatin was immunoprecipitated with antibody of ATF3 (Cell Signaling Technology, 18,665) or normal rabbit IgG (Cell Signaling Technology, 2729) overnight. Antibody/antigen complexes were

recovered with Protein G agarose beads (Cell signaling technology, 9007) for 2 h at 4°C. Two sequential elutions were performed. Eluted chromatin was diluted 1:3 with lysis buffer, supplemented with 1% Triton X-100 (Sigma-Aldrich, 9036-19-5) and incubated with 3 mg of normal rabbit IgG or anti-ATF3 antibody, overnight at 4°C. The immunoprecipitated DNA was collected. Purified DNA was performed with ChIP-PCR. The amount of immunoprecipitated DNA in each sample was determined as the fraction of the input and normalized to the IgG control.

Half-life of mRNAs analysis

1×10^6 /mL MRC-5 cells were seeded in a six-well plate including the control group, TGFB1-induced group, si-*ELAVL1*-treated group. Cells in control group were treated with 5 µg/mL actinomycin D (Aladdin, A13142-5 mg) alone for 4 h. Cells in TGFB1-induced group were first treated with 5 µg/mL TGFB1 for 24 h, then co-treated with 5 µg/mL actinomycin D for 4 h. Cells in si-*ELAVL1*-treated group were first treated with 5 µg/mL TGFB1 for 24 h, then co-treated with 10 µg/mL si-*ELAVL1* for 24 h, finally co-treated with 5 µg/mL actinomycin D for 4 h. *EZH2*, *STAT1* and *FOXK1* levels were measured by qRT-PCR at actinomycin D treatment for different times. *GAPDH* was used as an internal standard.

ELAVL1 stability assay

MRC-5 cells were seeded in a 6-cm cell culture plate. Cycloheximide (HX-R, T181074-1 g) was added to the medium at a final concentration of 10 µg/mL, thereby inhibited the synthesis of ELAVL1 protein. After cycloheximide treatment for different times, MRC-5 cell was harvested. The levels of ELAVL1 and GAPDH (Affinity, AF7021) proteins were detected by western blot.

Ubiquitination analysis

Cell samples were lysed in NP-40 lysis buffer (Thermo Scientific, 85,124) at 4°C for 30 min. The cell lysates were first incubated with antibodies of ELAVL1 and control IgG at 4°C overnight, and then were incubated with protein A/G (Absin, F08D04) beads for 3 h at 4°C. The beads were washed for three times with NP-40 lysis buffer. Western blotting analysis was carried out against anti-ubiquitin antibody (Abcam, ab134953).

Dual-fluorescence mRFP-GFP-LC3 detection

MRC-5 cell samples were seeded in a 24-well plate. 3 µL Dual-fluorescence mRFP-GFP-LC3 virus stock solution (Hanbio Inc, Shanghai, China) was diluted in 250 µL 10% FBS MEM medium and added into each well. After hatching for 2 h, the MEM medium contained virus was removed and the fresh MEM medium without FBS was added. After hatching for 12 h, real time dynamic changes of cells were monitored

under the IncuCyte S3 (Essen BioScience, USA) instrument and images were collected using a confocal microscope.

Statistical analysis

Statistical analysis were performed using SPSS version 19.0 software. Data were presented as the mean \pm SD of at least three independent experiments. Unpaired Student's t test was used for experiments comparing two groups, whereas one-way ANOVA with Student-Newman-Keuls post hoc test was applied for experiments comparing three or more groups. Statistical significance was considered at $p < 0.05$.

Acknowledgments

This work was supported by the National Natural Science Foundation of China (81970064, 81870001, 82170085, 81670064, and 31670365), the Important Project of Research and Development of Shandong Province (2019GSF108040), and the Natural Science Foundation of Shandong Province (ZR2020MH009, ZR2020MH010, ZR2019PH101, ZR2018PH001).

Disclosure statement

No potential conflict of interest was reported by the author(s).

Funding

This work was supported by the National Natural Science Foundation of China [81970064]; National Natural Science Foundation of China [81870001]; National Natural Science Foundation of China [81670064]; National Natural Science Foundation of China [31670365]; National Science Foundation of Shandong Province [ZR2018PH001]; National Science Foundation of Shandong Province [ZR2020MH009]; National Science Foundation of Shandong Province [ZR2020MH010]; National Science Foundation of Shandong Province [ZR2019PH101]; Important Project of Research and Development of Shandong Province [2019GSF108040].

References

- [1] Raghu G, Remy-Jardin M, Myers JL, et al. Diagnosis of idiopathic pulmonary fibrosis. An official ATS/ERS/JRS/ALAT clinical practice guideline. *Am J Respir Crit Care Med.* 2018;198(5):e44–e68.
- [2] Raghu G. Idiopathic pulmonary fibrosis: shifting the concept to irreversible pulmonary fibrosis of many entities. *Lancet Respir Med.* 2019;7(11):926–929.
- [3] Sarropoulos I, Marin R, Cardoso-Moreira M, et al. Developmental dynamics of lncRNAs across mammalian organs and species. *Nature.* 2019;571(7766):510–514.
- [4] Guo CJ, Ma XK, Xing YH, et al. Distinct processing of lncRNAs contributes to non-conserved functions in stem cells. *Cell.* 2020;181(3):621–636.e22.
- [5] Hessels D, Klein GJ, van Oort I, et al. DD3(PCA3)-based molecular urine analysis for the diagnosis of prostate cancer. *Eur Urol.* 2003;44(1):8–15.
- [6] Dallner OS, Marinis JM, Lu YH, et al. Dysregulation of a long noncoding RNA reduces leptin leading to a leptin-responsive form of obesity. *Nat Med.* 2019;25(3):507–516.
- [7] Liang H, Pan Z, Zhao X, et al. LncRNA PFL contributes to cardiac fibrosis by acting as a competing endogenous RNA of let-7d. *Theranostics.* 2018;8(4):1180–1194.

- [8] Xiao T, Zou Z, Xue J, et al. LncRNA H19-mediated M2 polarization of macrophages promotes myofibroblast differentiation in pulmonary fibrosis induced by arsenic exposure. *Environ Pollut.* **2021**;268(Pt A):115810.
- [9] Feng M, Tang PM, Huang XR, et al. TGF- β mediates renal fibrosis via the Smad3-ErbB4-IR long noncoding RNA axis. *Mol Ther.* **2018**;26(1):148–161.
- [10] Zhang S, Chen H, Yue D, et al. Long non-coding RNAs: Promising new targets in pulmonary fibrosis. *J Gene Med.* **2021**;23(3):e3318.
- [11] Song X, Xu P, Meng C, et al. lncITPF promotes pulmonary fibrosis by targeting hnRNP-L depending on its host gene ITGBL1. *Mol Ther.* **2019**;27(2):380–393.
- [12] Liu H, Wang B, Zhang J, et al. A novel lnc-PCF promotes the proliferation of TGF- β 1-activated epithelial cells by targeting miR-344a-5p to regulate map3k11 in pulmonary fibrosis. *Cell Death Dis.* **2017**;8(10):e3137.
- [13] Chang L, Zhou D, Luo S. Novel lncRNA LINC00941 promotes proliferation and invasion of colon cancer through activation of MYC. *Onco Targets Ther.* **2021**;14:1173–1186.
- [14] Liu H, Zhao X, Xiang J, et al. Interaction network of coexpressed mRNA, miRNA, and lncRNA activated by TGF-beta1 regulates EMT in human pulmonary epithelial cell. *Mol Med Rep.* **2017**;16(6):8045–8054.
- [15] Li Z, Schulz MH, Look T, et al. Identification of transcription factor binding sites using ATAC-seq. *Genome Biol.* **2019**;20(1):45.
- [16] Lan Y, Xiao X, He Z, et al. Long noncoding RNA OCC-1 suppresses cell growth through destabilizing HuR protein in colorectal cancer. *Nucleic Acids Res.* **2018**;46(11):5809–5821.
- [17] Nakahira K, Pabon Porras MA, Choi AM. Autophagy in pulmonary diseases. *Am J Respir Crit Care Med.* **2016**;194(10):1196–1207.
- [18] Mauthe M, Orhon I, Rocchi C, et al. Chloroquine inhibits autophagic flux by decreasing autophagosome-lysosome fusion. *Autophagy.* **2018**;14(8):1435–1455.
- [19] Füllgrabe J, Klionsky DJ, Joseph B. The return of the nucleus: transcriptional and epigenetic control of autophagy. *Nat Rev Mol Cell Biol.* **2014**;15(1):65–74.
- [20] Bowman CJ, Ayer DE, Dynlacht BD. Foxk proteins repress the initiation of starvation-induced atrophy and autophagy programs. *Nat Cell Biol.* **2014**;16(12):1202–1214.
- [21] Ambjørn M, Ejlerskov P, Liu Y, et al. IFN β /interferon-beta-induced autophagy in MCF-7 breast cancer cells counteracts its proapoptotic function. *Autophagy.* **2013**;9(3):287–302.
- [22] Chen H, Tu SW, Hsieh JT. Epigenetic regulation of autophagy by the methyltransferase EZH2 through an MTOR-dependent pathway. *Autophagy.* **2015**;11(12):2309–2322.
- [23] McEwan DG, Popovic D, Gubas A, et al. PLEKHM1 regulates autophagosome-lysosome fusion through HOPS complex and LC3/GABARAP proteins. *Mol Cell.* **2015**;57(1):39–54.
- [24] Yu M, Jiang Y, Feng Q, et al. DRAM1 protects neuroblastoma cells from oxygen-glucose deprivation/reperfusion-induced injury via autophagy. *Int J Mol Sci.* **2014**;15(10):19253–19264.
- [25] Zeng Y, Du WW, Wu Y, et al. A circular RNA binds to and activates AKT phosphorylation and nuclear localization reducing apoptosis and enhancing cardiac repair. *Theranostics.* **2017**;7(16):3842–3855.
- [26] Goodall GJ, Wickramasinghe VO. RNA in cancer. *Nat Rev Cancer.* **2021**;21(1):22–36.
- [27] Statello L, Guo CJ, Chen LL, et al. Gene regulation by long non-coding RNAs and its biological functions. *Nat Rev Mol Cell Biol.* **2021**;22(2):96–118.
- [28] Liu W, Wang Z, Liu L, et al. LncRNA Malat1 inhibition of TDP43 cleavage suppresses IRF3-initiated antiviral innate immunity. *Proc Natl Acad Sci U S A.* **2020**;117(38):23695–23706.
- [29] Zhang Y, Li Y, Hu Q, et al. The lncRNA H19 alleviates muscular dystrophy by stabilizing dystrophin. *Nat Cell Biol.* **2020**;22(11):1332–1345.
- [30] Yu CF, Xiao YL, Liu T, et al. c-Myc inactivation of p53 through the pan-cancer lncRNA MILIP drives cancer pathogenesis. *Nat Commun.* **2020**;11(1):4980.
- [31] Zhang J, Li Z, Liu L, et al. Long noncoding RNA TSLNC8 is a tumor suppressor that inactivates the interleukin-6/STAT3 signaling pathway. *Hepatology.* **2018**;67(1):171–187.
- [32] Zhang E, Han L, Yin D, et al. H3K27 acetylation activated-long non-coding RNA CCAT1 affects cell proliferation and migration by regulating SPRY4 and HOXB13 expression in esophageal squamous cell carcinoma. *Nucleic Acids Res.* **2017**;45(6):3086–3101.
- [33] Xie JJ, Jiang YY, Jiang Y, et al. Super-Enhancer-Driven long non-coding RNA LINC01503, regulated by TP63, is over-expressed and oncogenic in squamous cell carcinoma. *Gastroenterology.* **2018**;154(8):2137–2151.e1.
- [34] Fukushima K, Satoh T, Sugihara F, et al. Dysregulated expression of the nuclear exosome targeting complex component Rbm7 in nonhematopoietic cells licenses the development of fibrosis. *Immunity.* **2020**;52(3):542–556.e13.
- [35] Liu P, Luo G, Dodson M, et al. The NRF2-LOC344887 signaling axis suppresses pulmonary fibrosis. *Redox Biol.* **2021**;38:101766.
- [36] Cui H, Banerjee S, Guo S, et al. Long noncoding RNA Malat1 regulates differential activation of macrophages and response to lung injury. *JCI Insight.* **2019**;4(4):e124522.
- [37] Savary G, Dewaeles E, Diazi S, et al. The long noncoding RNA DNM3OS is a reservoir of fibromiRs with major functions in lung fibroblast response to TGF- β and pulmonary fibrosis. *Am J Respir Crit Care Med.* **2019**;200(2):184–198.
- [38] Jiang D, Liang J. A long noncoding RNA links TGF- β signaling in lung fibrosis. *Am J Respir Crit Care Med.* **2019**;200(2):123–125.
- [39] Zhao X, Sun J, Chen Y, et al. lncRNA PFAR promotes lung fibroblast activation and fibrosis by targeting miR-138 to regulate the YAP1-Twist axis. *Mol Ther.* **2018**;26(9):2206–2217.
- [40] Huang C, Liang Y, Zeng X, et al. Long noncoding RNA FENDRR exhibits antifibrotic activity in pulmonary fibrosis. *Am J Respir Cell Mol Biol.* **2020**;62(4):440–453.
- [41] Du Y, Hao X, Liu X. Low expression of long noncoding RNA CDKN2B-AS1 in patients with idiopathic pulmonary fibrosis predicts lung cancer by regulating the p53-signaling pathway. *Oncol Lett.* **2018**;15(4):4912–4918.
- [42] Li X, Yu T, Shan H, et al. lncRNA PFAL promotes lung fibrosis through CTGF by competitively binding miR-18a. *FASEB J.* **2018**;32(10):5285–5297.
- [43] Li C, Wang Z, Zhang J, et al. Crosstalk of mRNA, miRNA, lncRNA, and circRNA and their regulatory pattern in pulmonary fibrosis. *Mol Ther Nucleic Acids.* **2019**;18:204–218.
- [44] Levine B, Kroemer G. Biological functions of autophagy genes: a disease perspective. *Cell.* **2019**;176(1–2):11–42.
- [45] Dong X, Yang Y, Zou Z, et al. Sorting nexin 5 mediates virus-induced autophagy and immunity. *Nature.* **2021**;589(7842):456–461.
- [46] Racanelli AC, Kikkers SA, Choi AMK, et al. Autophagy and inflammation in chronic respiratory disease. *Autophagy.* **2018**;14(2):221–232.
- [47] Jessop F, Hamilton RF, Rhoderick JF, et al. Autophagy deficiency in macrophages enhances NLRP3 inflammasome activity and chronic lung disease following silica exposure. *Toxicol Appl Pharmacol.* **2016**;309:101–110.
- [48] Abdel Fattah E, Bhattacharya A, Herron A, et al. Critical role for IL-18 in spontaneous lung inflammation caused by autophagy deficiency. *J Immunol.* **2015**;194(11):5407–5416.
- [49] Mi S, Li Z, Yang HZ, et al. Blocking IL-17A promotes the resolution of pulmonary inflammation and fibrosis via TGF-beta1-dependent and -independent mechanisms. *J Immunol.* **2011**;187(6):3003–3014.
- [50] Han R, Ji X, Rong R, et al. MiR-449a regulates autophagy to inhibit silica-induced pulmonary fibrosis through targeting Bcl2. *J Mol Med (Berl).* **2016**;94(11):1267–1279.
- [51] Kobayashi K, Araya J, Minagawa S, et al. Involvement of PARK2-mediated mitophagy in idiopathic pulmonary fibrosis pathogenesis. *J Immunol.* **2016**;197(2):504–516.

- [52] Luo Y, Zheng S, Wu Q, et al. Long noncoding RNA (lncRNA) EIF3J-DT induces chemoresistance of gastric cancer via autophagy activation. *Autophagy*. 2021;17(12):4083–4101.
- [53] Wu Q, Ma J, Wei J, et al. lncRNA SNHG11 promotes gastric cancer progression by activating the Wnt/ β -Catenin pathway and oncogenic autophagy. *Mol Ther*. 2021;29(3):1258–1278.
- [54] Wang L, Yang J, Wang HN, et al. lncRNA BCYRN1-induced autophagy enhances asparaginase resistance in extranodal NK/T-cell lymphoma. *Theranostics*. 2021;11(2):925–940.
- [55] Xu T, Yan W, Wu Q, et al. MiR-326 inhibits inflammation and promotes autophagy in silica-induced pulmonary fibrosis through targeting TNFSF14 and PTBP1. *Chem Res Toxicol*. 2019;32(11):2192–2203.
- [56] Simion V, Zhou H, Haemmig S, et al. A macrophage-specific lncRNA regulates apoptosis and atherosclerosis by tethering HuR in the nucleus. *Nat Commun*. 2020;11(1):6135.
- [57] Li B, Chng WJ. EZH2 abnormalities in lymphoid malignancies: underlying mechanisms and therapeutic implications. *J Hematol Oncol*. 2019;12(1):118.
- [58] Duke KS, Taylor-Just AJ, Ihrie MD, et al. STAT1-dependent and -independent pulmonary allergic and fibrogenic responses in mice after exposure to tangled versus rod-like multi-walled carbon nanotubes. *Part Fibre Toxicol*. 2017;14(1):26.
- [59] Sukonina V, Ma H, Zhang W, et al. FOXK1 and FOXK2 regulate aerobic glycolysis. *Nature*. 2019;566(7743):279–283.